STM JOURNALS

Journal of
Modern Chemistry &
Chemical Technology

ISSN: 2229-6999 (Online)
ISSN: 2321-5208 (Print)
Volume 16, Issue 2, 2025
May–August
DOI (Journal): 10.37591/JoMCCT

https://journals.stmjournals.com/jomcct

Research JoMCCT

Role of Electron Donors in $MgCl_2$ Supported Ziegler-Natta Catalysis: DFT Approach

Jugal Kumawat[1], Parthiv Trivedi[2], Virendra Kumar Gupta[3,*]

Abstract

An insight into the nature of carbonate-based electron donors in high-activity $MgCl_2$ supported Ziegler-Natta (Z-N) catalysts has been studied and compared with conventional phthalate and diether systems by employing density functional theory (DFT) calculations. In the catalyst activation (one of the important processes to produce the active catalyst sites), the conventional monometallic and recently characterized bimetallic ($TiCl_2$(Et)-Cl-$AlEt_2$) active site are studied in the presence/absence of electron donors. These active sites were further investigated for olefin polymerization mechanisms using internal donor (ID) and with/without external donor (ED), dicyclopentadiene(dimethoxy)silane (DCPDMS). The current study also reveals that adding an alkoxysilane ED in Z-N improves the regio- and stereoselective behaviour and molecular weight of the polymer. Also, noncovalent interactions (NCIs) between the donor and the $MgCl_2$ surface and/or titanium catalyst are significant in investigating the ID effect in Z-N. The hydrogen response for all the donor catalyst systems was also studied and compared with conventional diisobutyl phthalate (DIBP) and diether donors. Therefore, these chemical calculations provide useful insight in understanding the nature of active sites and olefin polymerization mechanisms in Z-N.

Keywords: Ziegler-Natta olefin polymerization, DFT, noncovalent interaction, regio- and stereoselectivity, ester/carbonate donors

INTRODUCTION

The biggest breakthrough after the discovery of Ziegler-Natta (Z-N) catalyst [1–4] was observed when $MgCl_2$ was introduced as catalyst support [5, 6], and different Lewis bases [7] were introduced as an electron donor in Z-N catalysis. These led to Z-N catalysts as one of the most important processes for polyolefin production. Over the years, numerous experimental and computational efforts have been made to understand different aspects of the Z-N catalyst system [8–25]. The advancement of Z-N catalyst described in the form of different generations, where each successive generation leads to improve the catalyst activity and stereoselectivity of the Ti-catalyst in propylene polymerization.

***Author for Correspondence**
Virendra Kumar Gupta
E-mail: virendrakumar.gupta@ril.com

[1]Postdoctoral Researcher, Department of Chemistry and Biochemistry, Brigham Young University, Provo 84604, Utah, United States
[2]Lead Scientist, Polymer Synthesis & Catalysis Group, Reliance Research and Development Centre, Reliance Industries Limited, Navi Mumbai, India
[3]Senior Vice President, Polymer Synthesis & Catalysis Group, Reliance Research and Development Centre, Reliance Industries Limited, Navi Mumbai, India

Received Date: January 06, 2025
Accepted Date: February 12, 2025
Published Date: February 20, 2025

Citation: Jugal Kumawat, Parthiv Trivedi, Virendra Kumar Gupta. Role of Electron Donors in $MgCl_2$ Supported Ziegler-Natta Catalysis: DFT Approach. Journal of Modern Chemistry & Chemical Technology. 2025; 16(2): 51–81p.

The Z-N catalyst comprises the various components such as (a) the $MgCl_2$ catalyst support, (b) the $TiCl_4$ catalyst precursor, (c) the AlR_3, (R= alkyl group) catalyst activator, and (d) the Lewis base "donor". The most commonly used electron donors are: (i) internal donors (ID): donors added during the catalyst preparation, e.g., ethyl benzoate (*eb*) [9, 10, 26, 27], phthalates [28, 16, 29–32],

diethers [16, 30–35], succinate [32, 36, 37], and tetrahydrofuran (THF) [38, 39]; (ii) external donors (ED): the donors added during or after the alkylation, e.g., alkoxysilane [40–42]. Among all, the structural change in electron donors played a vital role in Z-N catalysts. Therefore, recent generations, especially the 4th, 5th, and 6th, differ by the nature of different electron donors such as phthalate, diether, and succinates. The main role of the donor is to sit beside the active titanium centre on the $MgCl_2$ surface and thereby influence the catalyst activity [43], regio- and stereoselectivity of the titanium catalyst [43–46] and hydrogen response [34, 43].

In 2011, Coalter *et al.* have reported a series of carbonate-based Z-N catalyst systems for propylene polymerization [46]. The performance of these carbonate-based donors is significantly higher compared to the 4th, 5th, and 6th generation catalyst systems. Currently, in Z-N, the major challenge is developing even more robust and advanced donors for the next generation catalyst with respect to the existing donors because of its high demand and sustainability. In this regard, recently, many donor catalyst systems have been examined by various groups such as bio-derived diesters by Taniike *et al.* [47], bioderived maleic rosinate tri-n-butyl and maleic rosinate tri-n-octyl-based donors by Huang *et al.* [45], multicarbonate-based donor by Gupta *et al*. [48], polyethylenimines-based multidentate donors by Pakkanen *et al.* [49], salicylate-based donors by Parasuk *et al.* [50] etc. to develop an effective Z-N catalyst system. To some extent, researchers have achieved the desired catalyst performance using a different range of electron donors; but these are still less effective than the carbonate-based donor catalysts as reported by Coalter *et al*. [46], to develop advanced robust catalyst systems, the structural property relationship of these carbonates and other existing donor-based catalyst systems need to be explored [43–45]. The systematic understanding of these donors, especially on surface stabilization, nature of active sites, and olefin polymerization, including termination processes, is still limited. Therefore, the detailed fundamental understanding of these existing donors in terms of different functional groups and the incorporation of noncovalent interactions (NCIs) are worth exploring in Z-N. Furthermore, NCIs played an important role in influencing the catalyst performance confirmed in many other catalysis studies such as asymmetric hydroformylation [51], catalytic asymmetric Heck-Matsuda Arylation [51], organocatalytic Michael addition [52], cycloisomerization [53], and other catalytic reactions [54]. Therefore, incorporation of these weak interactions in Z-N would help to understand and develop the advanced catalyst systems. Though, there are numerous studies on the nature of active titanium species in Z-N and their performance during olefin polymerization, researchers are exploring fundamental understanding of the catalyst activation process and how the inactive Ti(IV) species converts into the active Ti(III) catalyst sites. Few studies reported on the catalyst activation process where the AlR_3 species played an important role [9, 11, 55]; Cavallo *et al.* [11] have explained the systematic catalyst activation mechanism through two consecutive steps: (i) Ti-Cl bond cleavage and (ii) the transalkylation, where the transfer of one alkyl group from aluminium to the titanium and one chlorine atom from titanium to the aluminium species occur simultaneously.

The "dormant" bimetallic ($Cl_2Ti(Et)$-Cl-$AlEt_2$) active species in the absence of electron donor for ethylene polymerization [55]. In Z-N, mainly internal and/or external donor-based catalyst systems are considered for olefin polymerization. So, their effect on activation could be important to understand the Z-N activation process. Kumawat *et al.* have shown the effect of various internal donors on the monometallic catalyst activation mechanism [9], however, the effect of internal and/or external donors on the catalyst activation process, especially on bimetallic active site and its comparison with the monometallic active site could be explored. Since the electron donors are present in the Z-N system during the time of the catalyst activation [38, 56, 57]. Thus, a systematic fundamental understanding of the effect of electron donors on the catalyst activation mechanism and their (active sites) role in olefin polymerization is worth exploring in Z-N catalyst system. Therefore, we have reported DFT calculations that revealed the effect of different carbonate- and ester-based donors on donor coordination, catalyst activation, and olefin (ethylene and propylene) polymerization, where NCIs played an important role. For this study, different carbonate- (Donor_1, Donor_2, and Donor_3), ester-based (Donor_4), and phthalate donors are considered (Figure 1).

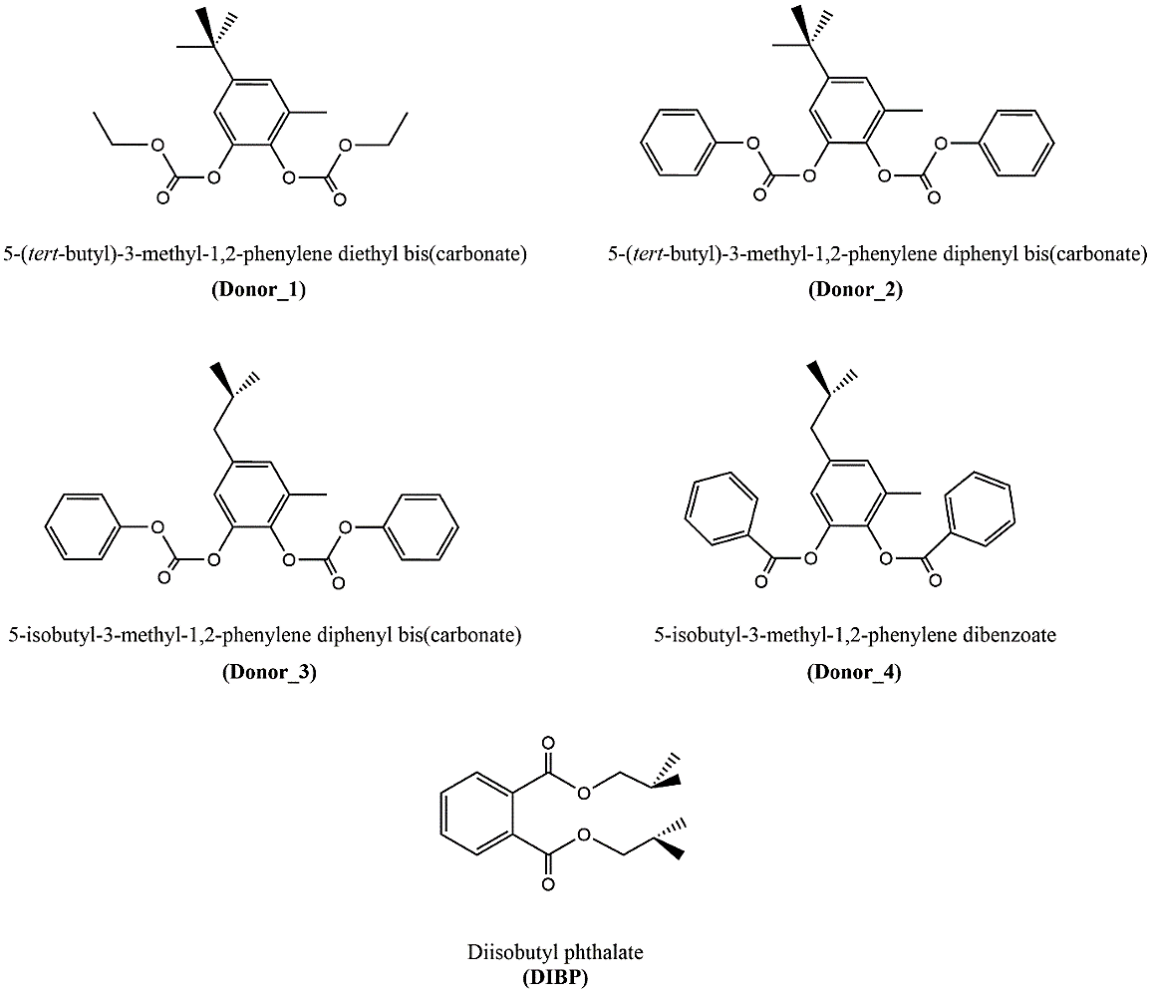

Figure 1. Different carbonate- and ester-based donors used in this study.

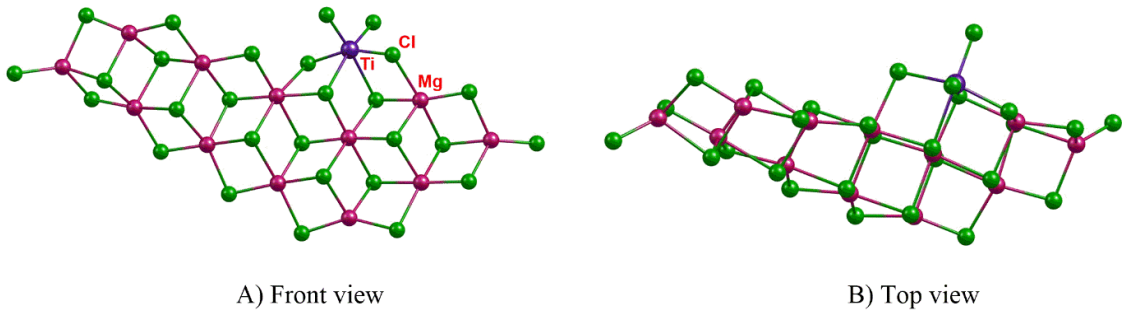

Figure 2. Optimized $MgCl_2$ model employed in this study.

The mono- and bimetallic active sites are used for olefin polymerization. To investigate their effectiveness, a comparative study with conventional donor families was also performed. In addition, the effect of donors (ID and/or ED) on the regio- and stereoselective behaviour of the Ti-catalyst for propylene polymerization was studied. Furthermore, the response of hydrogen as a chain terminating agent was also considered for Donor_1, Donor_2, Donor_3, and Donor_4 and compared with conventional phthalate and diether donors.

COMPUTATIONAL DETAILS

The Turbomole 7.0 suite of the program is considered for all the intermediates and transition state optimizations [58]. For these calculations, the Becke and Perdew (BP86) functional [59–61], followed

by single-point calculations with M06 [62]/Def2TZVPP is carried out in Gaussian16 [63]. The resolution of identity (RI) [64] along with the multipole accelerated resolution of identity (MARIJ) [65] approximations have been employed for an accurate and efficient treatment of the electronic Coulomb term in the DFT calculations. The Gibbs free energy (ΔG) values that have been calculated in this study, mainly contain the entropic, zero-point energy, and internal energy. For the correct transition state, care has been taken to ensure the single imaginary frequency with correct normal vibration mode. Intrinsic reaction coordinates (IRC) calculations were also performed to verify the transition state connections with energy surface [66]. The quasi-Newton-Josephson method was considered for the transition state, which is based on the restricted second-order method, which employs the Hessian shift parameters. In this study, the unrestricted method was employed.

RESULTS AND DISCUSSION

Donor Coordination to $TiCl_4$ Supported $MgCl_2$ Surface

Initially, the coordination of carbonate- and ester-based donors to the $TiCl_4$ supported $MgCl_2$ surface was investigated (Figure 1). For this study, the "$MgCl_2$ model" system was considered, which was originally proposed by Cavallo *et al.* (Figure 2) [13]. This model is a combination of (110) and (104) lateral cuts. For all the donor cases, the mono-, chelate-, and bridge-coordination possibilities to the $MgCl_2$ surface were investigated. Among all, the bridge-coordination was found to be more favourable (Table 1). The $MgCl_2$ surface has five-coordinated (104) lateral cuts, therefore, the binding of the donor to the $MgCl_2$ surface through two oxygen atoms to single magnesium (as a chelate coordination) leads to detachment of one of the Mg-Cl bond (due to more than six coordination on single magnesium atom) resulted in destabilizing the $MgCl_2$ surface compared to the bridge-coordination. The optimized structure of Donor_4 coordination to the $MgCl_2$ surface through chelate-coordination mode is shown in Figure S1 as a representative example. Table 1 compiles all the coordination energies for all the donors. The bridge-coordination energies are 34.1, 34.2, 33.1 and 34.0 kcal/mol for the Donor_1, Donor_2, Donor_3 and Donor_4, respectively which is almost same for all the donor cases. Furthermore, to understand the effect of different electronic and steric factors on donor coordination, a modification in Donor_3 was studied where carbonate phenyl was replaced by cyclohexane, methyl and biphenyl group that stabilized the surface by 26.4, 29.1 and 34.0 kcal/mol. These results suggest that on increasing the steric bulk (cyclohexane), decrease in the surface stabilization was observed and increasing the electronics away from the carbonate group does not improve the stabilization much. These donors stabilized the $MgCl_2$ surface more than two folds compared to the DIBP donor (15.7 kcal/mol). Carbonate donors are more electronically rich as well as have a favourable interaction with $MgCl_2$ surface that facilitate in stabilizing the Z-N system.

Table 1. Donor coordination to the $TiCl_4$ supported $MgCl_2$ surface.

S.N.	Donor	Coordination mode	ΔG (kcal/mol)
1	Donor_1	Mono	–14.5
		Bridge	–34.1
		Chelate	–16.3
2	Donor_2	Mono	–19.0
		Bridge	–34.2
		Chelate	–16.5
3	Donor_3	Mono	–19.0
		Bridge	–33.1
		Chelate	–16.8
4	Donor_4	Mono	–19.3
		Bridge	–34.0
		Chelate	–22.9
5	DIBP	Bridge	–15.7

Catalyst Activation

Initially, the Ti(IV)Cl_4 was adsorbed on the $MgCl_2$ surface and performed the six-coordinated octahedral complex [9, 67, 68], which is one of the most accepted structures in Z-N. The addition of $AlEt_3$ species into the Z-N starts the activation process. In this section, a detailed catalyst activation mechanism, where the inactive Ti(IV)Cl_4 catalyst converts into the active catalyst sites (Ti(III)Cl_2(Et) and/or Ti(III)Cl_2(Et).(Cl)$AlEt_2$) [69] is discussed using $AlEt_3$. Moreover, the effect of donors (ID and ED) on the catalyst activation mechanism was also investigated by coordinating to the $MgCl_2$ surface. This catalyst activation mechanism was investigated in two consecutive steps: a) Ti-Cl bond cleavage and (ii) the trans alkylation step [9, 10]. The nomenclature that has been given in Figures are **1**, **2**, **3**, and **4** for the without donor (*wd*), Donor_1, Donor_2, Donor_1 with alkoxysilane and Donor_2 with an alkoxysilane, respectively.

Figure 3 shows the free energy profile for the catalyst activation mechanism using without donor (*wd*) and ID (Donor_1 and Donor_2). As mentioned above, the titanium complex is present in the octahedral form on the $MgCl_2$ surface. Initially, in the first step (Ti-Cl bond cleavage), the homolytic cleavage of one of the Ti-Cl bond takes place in the presence of the $AlEt_3$ species. This step leads to the two species, one is an intermediate having a vacancy on the titanium metal centre (**1'a**, **1a**, and **2a**), and the $AlEt_3Cl$ radical (Figures 3 and 4). For this step, only the thermodynamics of a reaction was considered as reported by other previous studies [9, 10]. This step is endergonic in nature by 21.0, 19.1, and 16.7 kcal/mol for without donor (*wd)*, Donor_1, and Donor_2 catalyst systems, respectively. In this step, Donor_2 is comparatively lesser endergonic with respect to Donor_1. The reason is that in the case of Donor_2, the phenyl ring of the donor is interacting to the titanium centre through metal-p interaction to the vacant site, which is helping in stabilizing the **2a** intermediate (Figure S2). Along with the Ti-Cl bond cleavage, donor displacement was also studied (Figure S3).

In the next step, as Figure 3 shows, another $AlEt_3$ moiety coordinates to the titanium and leads to the **1'b**, **1b**, and **2b** intermediates which is endergonic by 0.2, 2.3, and –0.9 kcal/mol. Afterwards, the **1'b**, **1b**, and **2b** intermediate rearrange and lead to the **1'c**, **1c**, and **2c** intermediate through a four-membered transition states, $\mathbf{TS_{1'b\text{-}1'c}}$, $\mathbf{TS_{1b\text{-}1c}}$, and $\mathbf{TS_{2b\text{-}2c}}$. The energy barriers for this conversion are 12.9, 15.9, and 19.4 kcal/mol for the without donor (*wd)*, Donor_1, and Donor_2, respectively. This step is the rate-determining step for the catalyst activation for all the systems. These energy barriers suggest that the reaction rate for the without donor (*wd*) case is slightly faster compared to IDs. Then, this (**1'c**, **1c**, and **2c**) intermediate leads to the **1'd**, **1d**, and **2d** bimetallic intermediate species through a four-membered transition state ($\mathbf{TS_{1'c\text{-}1'd}}$, $\mathbf{TS_{1c\text{-}1d}}$, and $\mathbf{TS_{2c\text{-}2d}}$), which is stabilized by 15.5, 8.7, and 13.4 kcal/mol at energy landscape (Figure 3). Recently, this bimetallic intermediate (**1'd**) is characterized [55] and claimed as a "dormant" active species for ethylene polymerization (Figures S4–8).

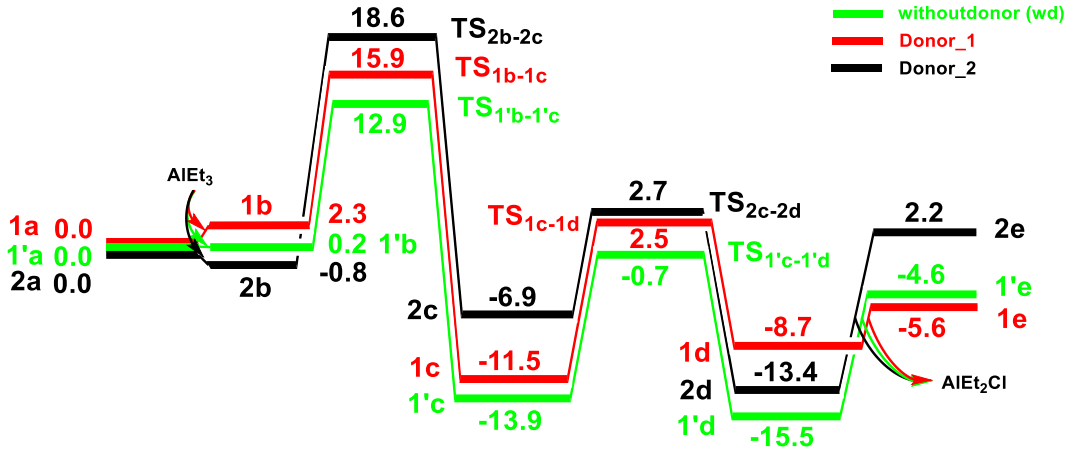

Figure 3. The free energy profile for the comparative study between without donor (*wd*), Donor_1, and Donor_2 for the trans alkylation step.

The energy barriers for the formation of this bimetallic species are 13.2, 13.9, and 9.6 kcal/mol for without donor (*wd)*, Donor_1, and Donor_2, respectively. For the *wd*, this barrier is comparable with previous barrier. The bimetallic intermediate further converts into the final conventional active titanium species (**1'e**, **1e**, and **2e)** and a $AlEt_2Cl$ species (Figure 3). The optimized transition state structures for the catalyst activation mechanism for the without donor (*wd*), Donor_1, and Donor_2 systems are shown in Figure 5. The formation of final conventional active titanium species is energetically favourable by 4.6, 5.6, and 2.2 (endergonic) kcal/mol with respect to the starting point on the energy landscape. However, this conventional active species is thermodynamically less favourable than the bimetallic "dormant" active species (Figure 3). The final product (**1'e**, **1e**, and **2e**) consists of an ethyl group on the titanium metal centre, which is the active catalyst species responsible for the chain growth in Z-N olefin polymerization catalyst. The Ti-Cl bond cleavage and trans alkylation results suggest that the Donor_1 and Donor_2 systems are slightly slower the catalyst activation process in $MgCl_2$ supported Z-N catalysis.

Based on the mechanism of without donor (*wd*) and ID (Donor_1, Donor_2) outlined in Figure 3, we also examined the catalyst activation mechanism by incorporating alkoxy silane ED (**3** and **4**) on Donor_1 and Donor_2 catalyst systems. Figure S5 shows the full energy landscape for the **3** and **4** catalyst systems. Here, alkoxy silane coordination to the $MgCl_2$ surface just beside the titanium opposite to ID is considered which stabilized the surface by 8.2 and 6.4 kcal/mol for the **3** and **4**, respectively. The Ti-Cl bond cleavage step is 17.3 and 14.0 kcal/mol endergonic in nature with respect to the **1** and **2** systems (19.1 and 16.7 kcal/mol). Figure S5 shows that for **3** and **4** also the first transalkylation step is the rate determining step and the barriers for this step are 15.5 and 22.4 kcal/mol. The final catalyst active sites are also exergonic in nature with respect to the starting points by 1.3 and 2.2 kcal/mol for catalyst **3** and **4**, respectively (Figures S5 and S6).

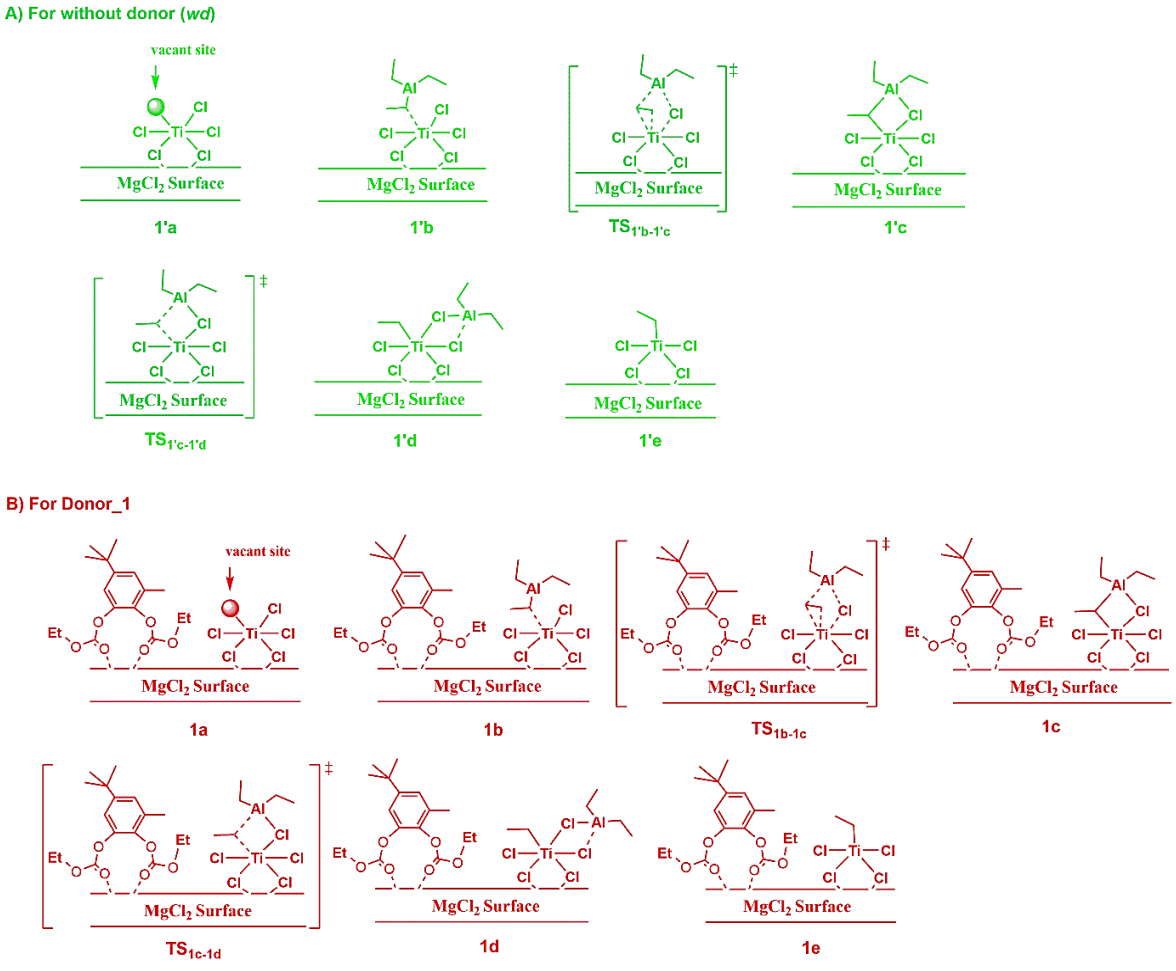

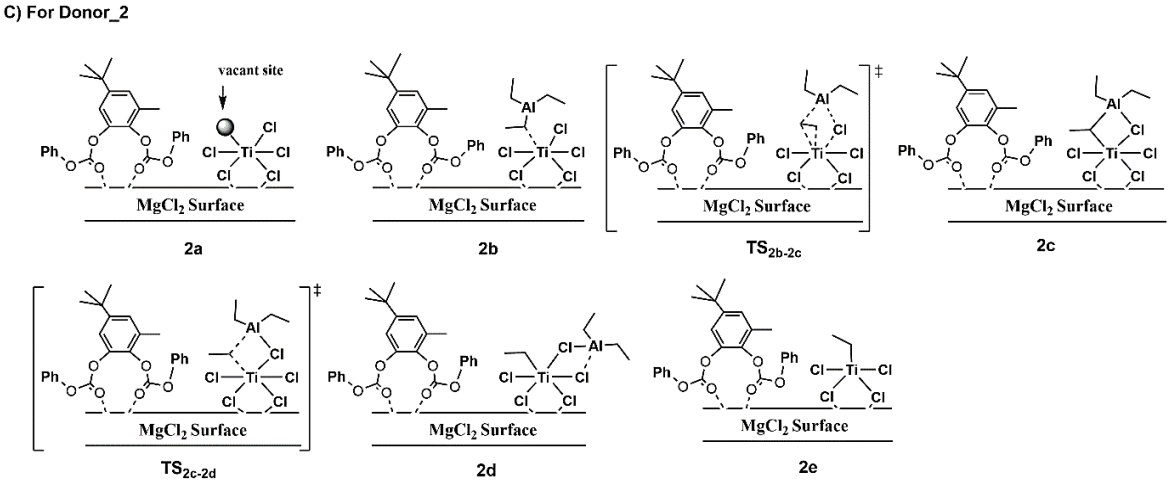

Figure 4. Different intermediate and transition state structures that are indicated in Figure 3.

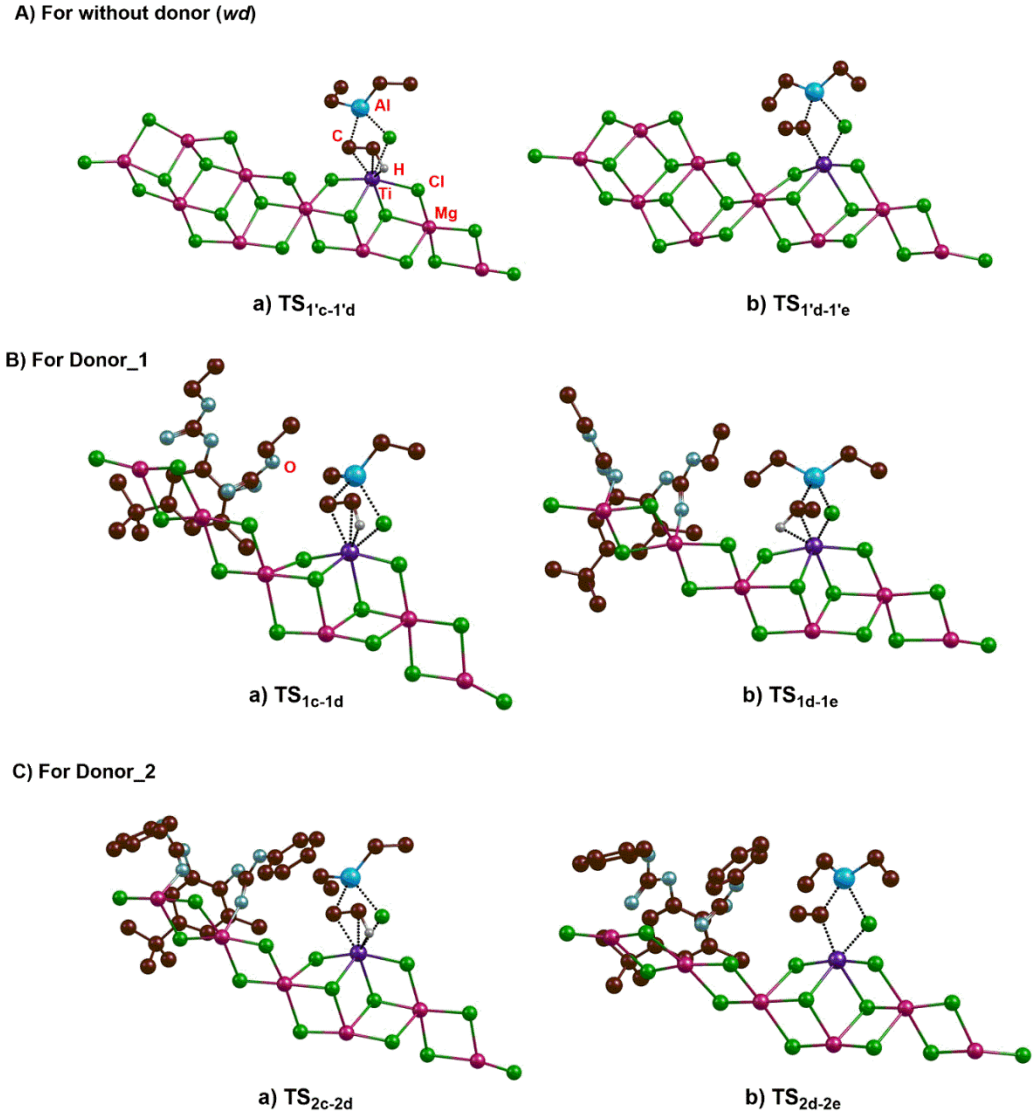

Figure 5. Optimized transition state structures for the trans alkylation step, for (A) without donor (*wd*), B) the Donor_1, and C) Donor_2 systems; all the $MgCl_2$ layers and hydrogen atoms are not shown for the clarity.

Overall, the catalyst activation mechanism was studied using without donor (*wd*), Donor_1, and Donor_2 in the presence/absence of alkoxysilane external donor (Table S1; for comparative study between **1'**, **1**, **2**, **3**, and **4** catalysts are shown in SI file). These results suggest that the presence of the donors (ID and ED) slows the activation process. And among ID and ED, the EDs even slowdown the activation process compared to IDs. These active sites are responsible for the olefin polymerization in Z-N (Figures S8–S10).

Ethylene Polymerization

The active catalyst species were observed during catalyst activation mechanism and considered for the ethylene polymerization. Here, mono- and bimetallic active sites are considered for the ethylene polymerization by following the Cossee-Arlmann mechanism [70]. Initially, the ethylene monomer approaches on the titanium centre in both the active sites and forms the π-complexation. For both the active species, the π-complexations are endergonic in nature by 1.5 and 12.5 kcal/mol.

The reason is that in the case of monometallic, the titanium has a five, coordinated with one vacant site, where the incoming monomer formed the stable octahedral complex (Figure 6). Whereas, in the case of bimetallic, the titanium already has a six-coordinated stable structure with no vacancy for the incoming monomer. Therefore, during the π-complexation, the titanium displaces one of the surface chlorine atoms, which leads to a distorted octahedral complex (Figure 6). Then, ethylene monomer inserts into the Ti-Et bond and leads to the Ti-C_4H_9 product through a four-membered insertion transition state. The energy barriers for this conversion are 7.9 and 25.1 kcal/mol for the mono- and bimetallic active sites. Along with insertion, a competitive chain transfer to monomer termination transition state is also studied and the barriers are 15.3 and 25.6 kcal/mol. The termination barrier is higher with respect to the insertion due to more sterically hindered six-membered transition state [70]. The optimized structures for π-complex and transition states are shown in Figure 6. The ΔX values (termination-insertion barrier) are 8.9 and 0.5 kcal/mol for the mono- and bimetallic active sites. Also, the energy barriers for the bimetallic active site are higher compared to the monometallic. Therefore, above results suggest that the conventional monometallic active site is more effective towards ethylene polymerization leading to high molecular weight polymer than the bimetallic active site, which only leads to oligomers or low molecular weight polymer.

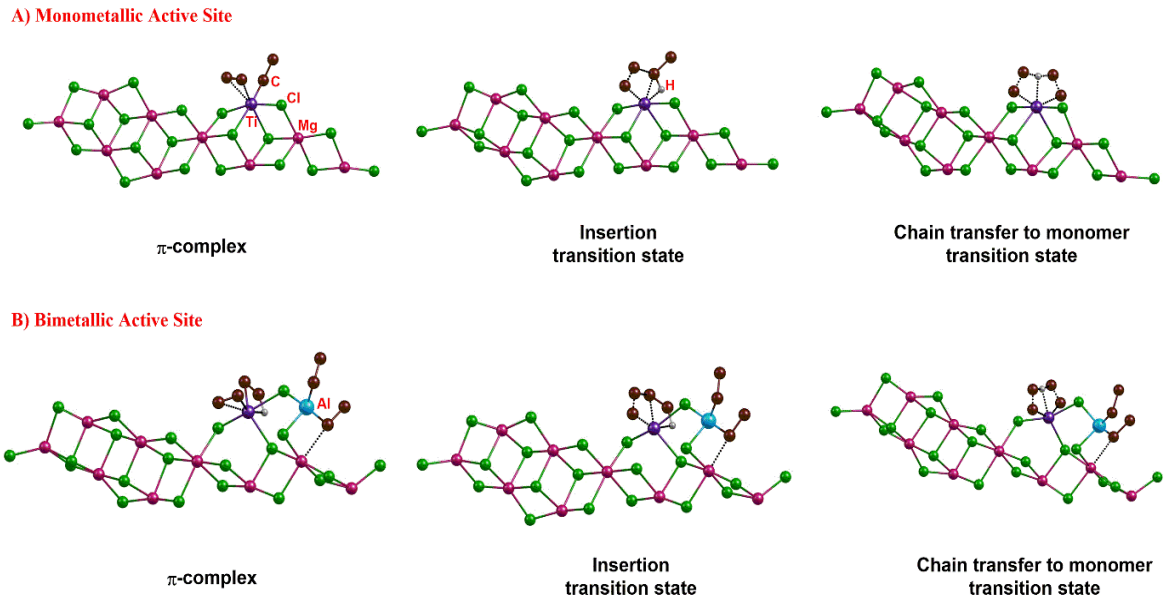

Figure 6. Optimized π-complex, insertion, and chain transfer to monomer transition state structures for ethylene polymerization using mono- and bimetallic active sites: All the $MgCl_2$ layer and hydrogen atoms are not shown for the purpose of clarity.

Effect of Donors on Ethylene Polymerization through Monometallic ($TiCl_2$-Et) Active Site

Figure 7 shows the effect of donor on ethylene polymerization. For this study, only the monometallic ($TiCl_2$-Et) active site was considered. Table 2 compiles all the polymerization steps (π-complexation, insertion, and termination transition state) energy values with all the donor catalyst systems. In case of Donor_3, p-complexation is exergonic due to less sterically hindered iso-butyl group near $MgCl_2$ layer and more favourable NCI interactions between both the phenyls and phenyl and titanium metal (Figure 9) (Table S1). For Donor_1, the insertion and termination barriers are higher due to absence of NCI interactions with respect to other donors (Figure 8). Table 2 shows the comparable ΔX values ~9.5 kcal/mol for all the donor catalyst systems which suggest that these donors lead to high molecular weight polymer compared to the existing DIBP (ΔX=6.5 kcal/mol) [48]. Furthermore, the effect of diverse electronic and steric factors on ethylene polymerization has also been considered by substituting different alkyl groups on the Donor_3.

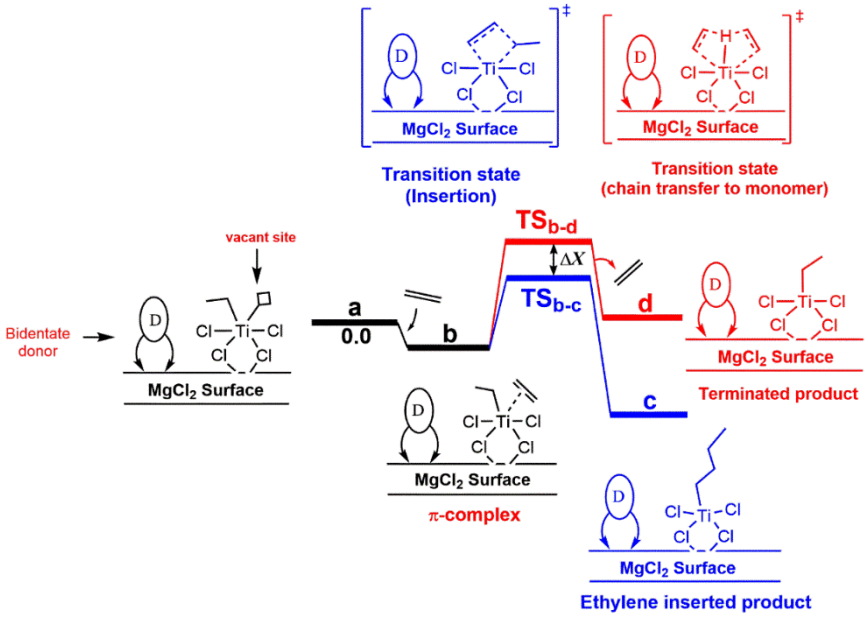

Figure 7. Energy profile for the insertion and termination (chain transfer to monomer) steps in ethylene polymerization.

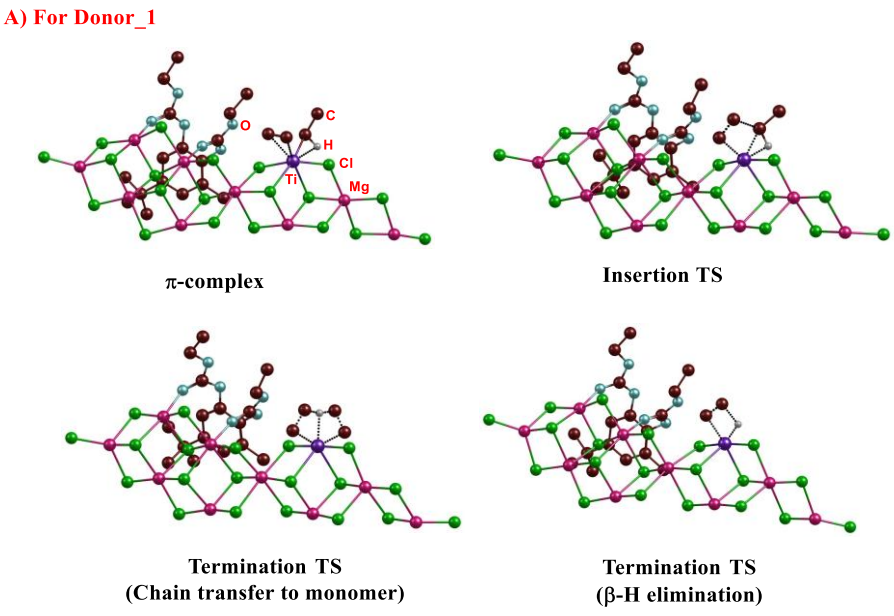

B) For Donor_2

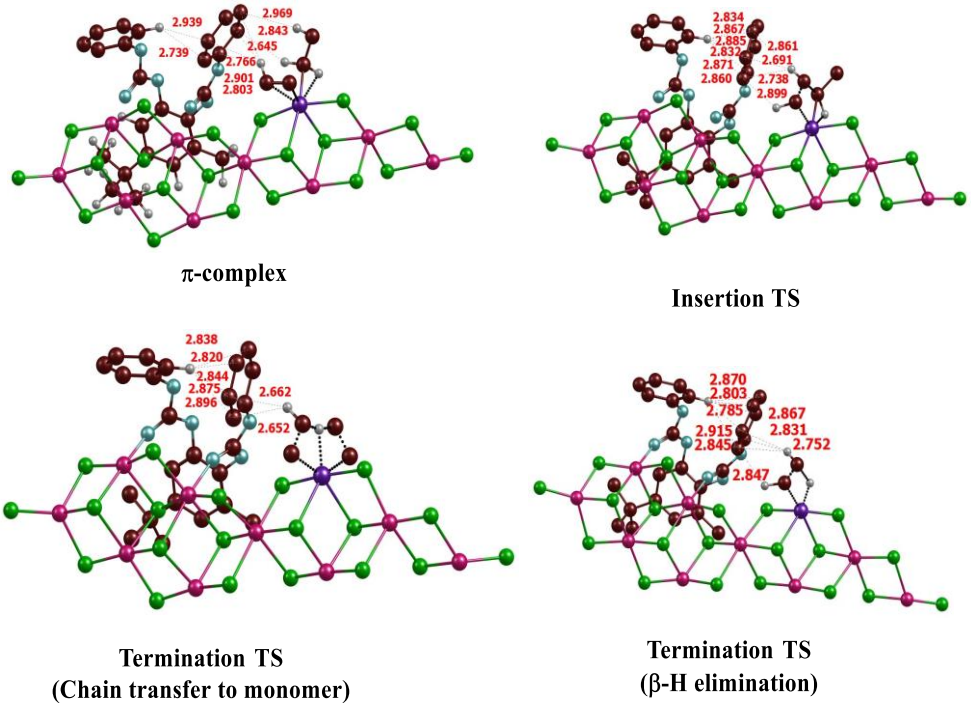

Figure 8. Optimized p-complexation and transition state (insertion and termination) structures for Donor_1 and Donor_2; all the $MgCl_2$ layer and hydrogen atoms are not shown for the clarity.

Table 2. Ethylene polymerization study using different internal donor catalyst systems.

Donor	**ΔG (kcal/mol)**				
	π–complex (b)	***Insertion barrier (TS_{b-c})***	***Termination***		***ΔX (Lower termination)–(Insertion barriers)***
			Chain transfer to monomer barrier (TS_{b-d})	*β–H elimination barrier (TS_a)*	
Donor_1	4.7	12.4	21.6	30.0	9.1
Donor_2	1.8	7.6	17.4	22.0	9.8
Donor_3	–4.4	7.5	17.2	18.0	9.7
Donor_4	1.5	8.3	17.7	21.3	9.4
DIBP [71]	–11.1	5.2	11.7	20.6	6.5

The effect of alkoxysilane external donor on ethylene polymerization compared to the lone internal donors has been investigated. For this study, Donor_1 and Donor_2 systems are considered. Table 3 compiles the p-complexation, and insertion and termination barriers for the alkoxysilane coordinated Donor_1 and Donor_2 catalyst systems.

Energy barriers for the chain transfer to the monomer are 23.4 and 22.3 kcal/mol, which is higher compared to the b-H elimination, 18.2 and 19.1 kcal/mol due to a more sterically constrained six-membered transition state with respect to less constrained four-membered transition state. The binding of alkoxysilane on the $MgCl_2$ surface blocks some of the space of the titanium centre, which hindered the insertion and termination process. The optimized transition state structures for the insertion and the termination steps are shown in Figure 10. The D*X* value suggest that the adding the alkoxysilane donors slightly reduces the molecular weight in ethylene polymerization.

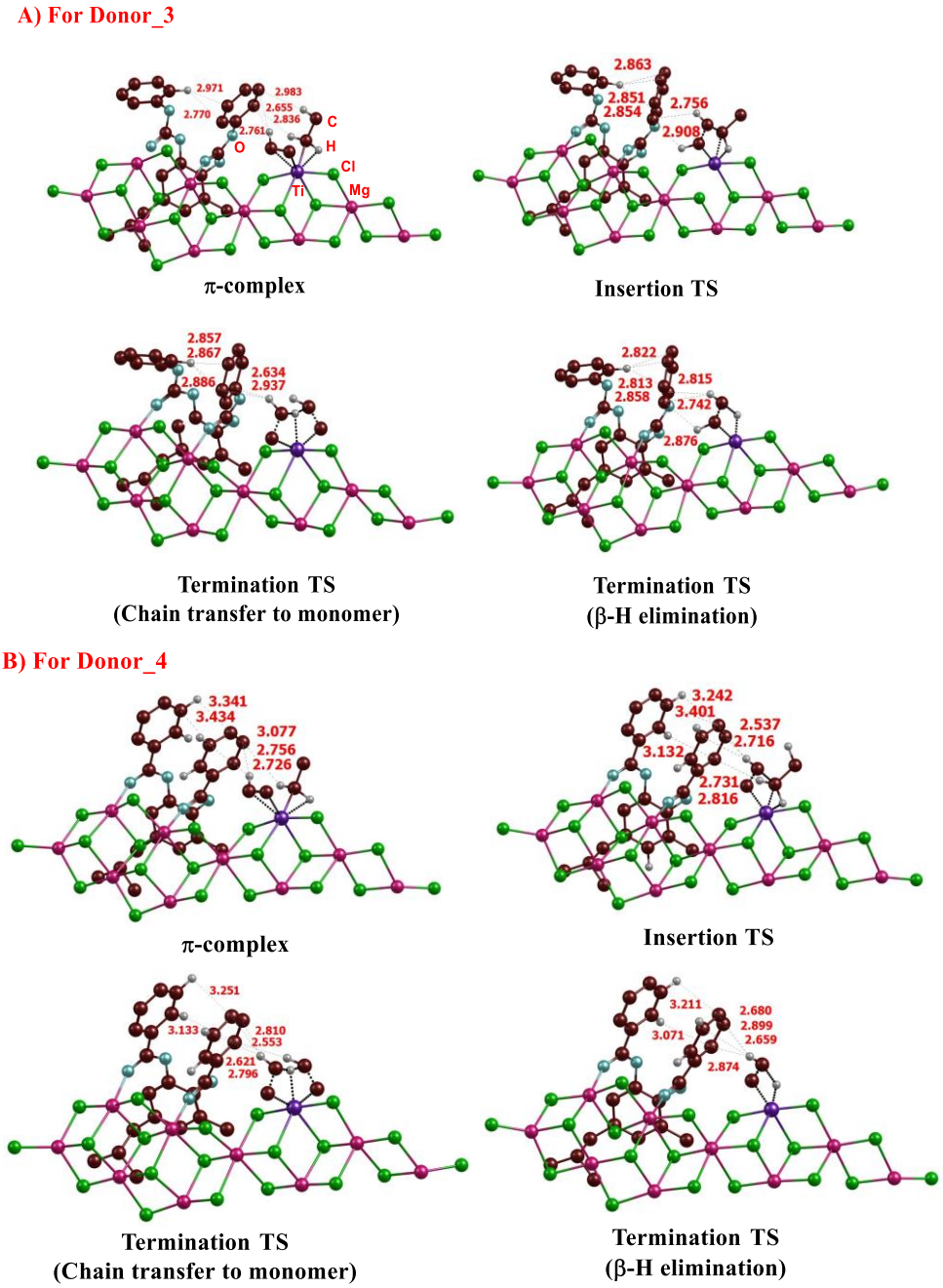

Figure 9. Optimized p-complexation and transition state (insertion and termination) structures for the Donor_3 and Donor_4; all the $MgCl_2$ layer and hydrogen atoms are not shown for the clarity.

Table 3. A comparative ethylene polymerization study between lone Donor_1 and Donor_2, and alkoxysilane containing Donor_1 and Donor_2 catalyst systems.

Donor catalyst system		**ΔG (kcal/mol)**				
		π–complex (b)	***Insertion (TS_{b-c})***	***Termination***		***ΔX (Lower termination)–(Insertion barriers)***
ID	ED			*Chain transfer to monomer (TS_{b-d})*	*β–H elimination*	
Donor_1	None	4.7	12.4	21.6	30.0	9.1
Donor_1	alkoxysilane	3.6	10.9	23.4	18.2	7.3
Donor_2	None	1.8	7.6	17.4	22.0	9.8
Donor_2	alkoxysilane	4.6	10.7	22.3	19.1	8.4

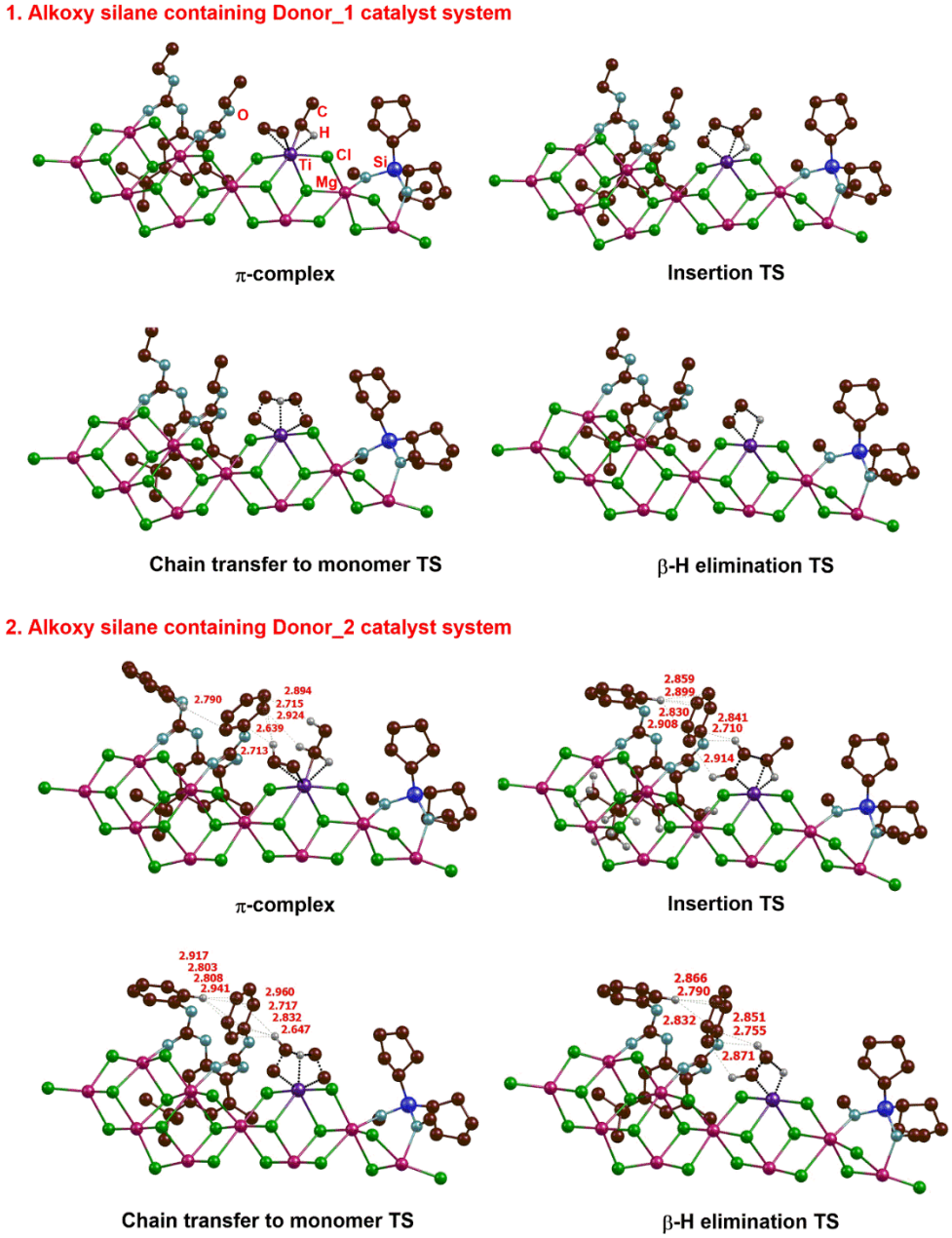

Figure 10. Optimized p–complexation and transition state structures for the insertion and the terminations steps using alkoxysilane containing Donor_1 and Donor_2 catalyst systems: all the $MgCl_2$ later and hydrogen atoms are not shown for clarity.

H_2 Response

In Z-N, H_2 molecules are usually introduced to terminate the polymer carbon chain from the titanium centre [71, 46, 72]. It has been observed that adding an electron donor improves the hydrogen response in Z-N [43]. Here, the H_2 response of Donor_1, Donor_2, Donor_3, and Donor_4 was investigated and compared with existing DIBP and diether. Initially, the H_2 molecule coordinates to the titanium centre and performed the s-complex in all the donor catalyst systems (Figure 11).

These coordination are less endergonic with Donor_2, Donor_3, and Donor_4 because of favourable interactions between ligand and titanium species (Table 4 and Figures S9 and S10). In the next step, the H_2 terminates the polymer chain by transferring one hydrogen to a carbon chain and another to the titanium metal centre through a four-membered transition state (Figure 11). These results indicate that

current donors have high hydrogen responses compared to DIBP and diether. Among DIBP and diether, the diether has better hydrogen response, which is in accord with the experimental findings [43, 44]. In all the carbonate donors, Donor_2 and Donor_3 have better hydrogen responses than the Donor_1 owing to NCIs, which is helping in stabilizing the s-complexes and transition states (Figures S9 and S10). The optimized s-complex and transition state structures are shown in Figures S9 and S10. These chemical calculations therefore indicate that carbonate donors exhibit a more effective hydrogen response compared to the existing phthalate and diether donors, with the ligand framework playing a key role in modulating their performance.

Propylene Polymerization

The regio- and stereoselectivity behaviour of the titanium catalyst on propylene polymerization has also been studied using Donor_1, Donor_2, Donor_3, and Donor_4. For all the cases, four different possibilities are considered for the insertion of a propylene monomer into the Ti-Et growing polymer chain. These possibilities are 1,2-*re*, 1,2-*si*, 2,1-*re*, and 2,1-*si*, depending upon the orientation of the methyl group of the propylene monomer (Scheme 1).

In propylene polymerization, the stereoselective nature of the polypropylene depends upon the chirality of the Ti-complex, and this chirality can be labelled as Λ or Δ [73]. For the sake of ease, the Λ configuration is considered for the octahedral titanium complex.

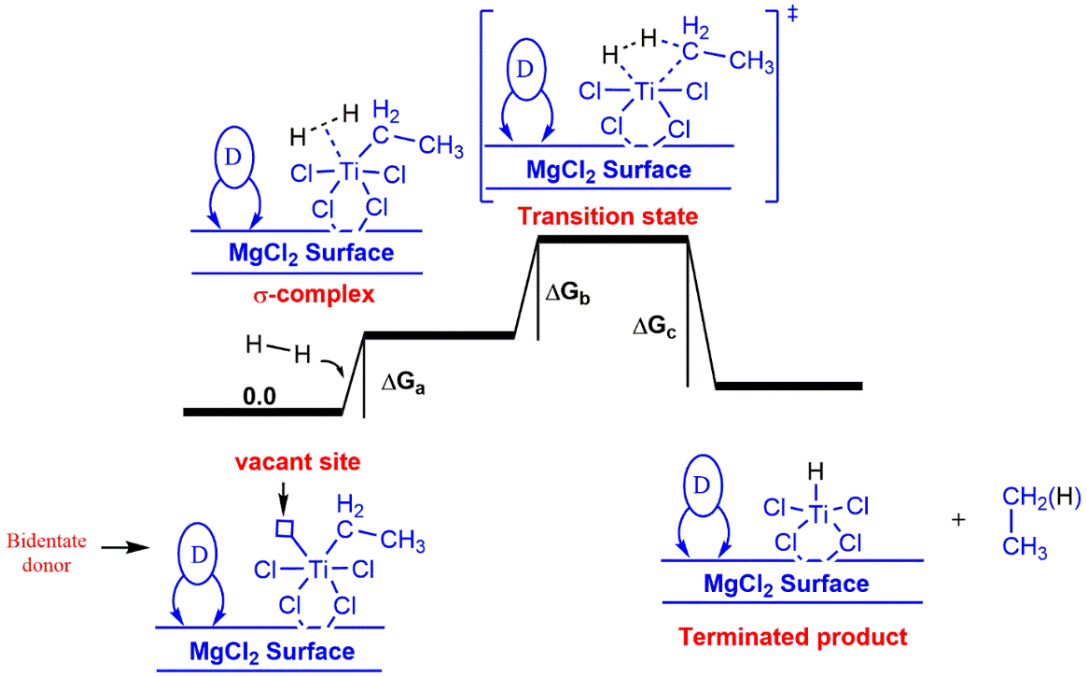

Figure 11. Energy profile for the hydrogen response.

Table 4. Effect of donors on hydrogen response.

Donor	DG (kcal/mol)			
	DG_a	DG_b	$DG_a + DG_b$	DG_c
Donor_1	12.3	6.9	19.2	–14.3
Donor_2	5.5	10.7	16.2	–16.0
Donor_3	3.2	7.9	11.1	–14.7
Donor_4	7.4	8.8	16.2	–15.7
DIBP	10.9	12.4	23.3	–21.8
Diether	10.4	7.9	18.3	–12.2

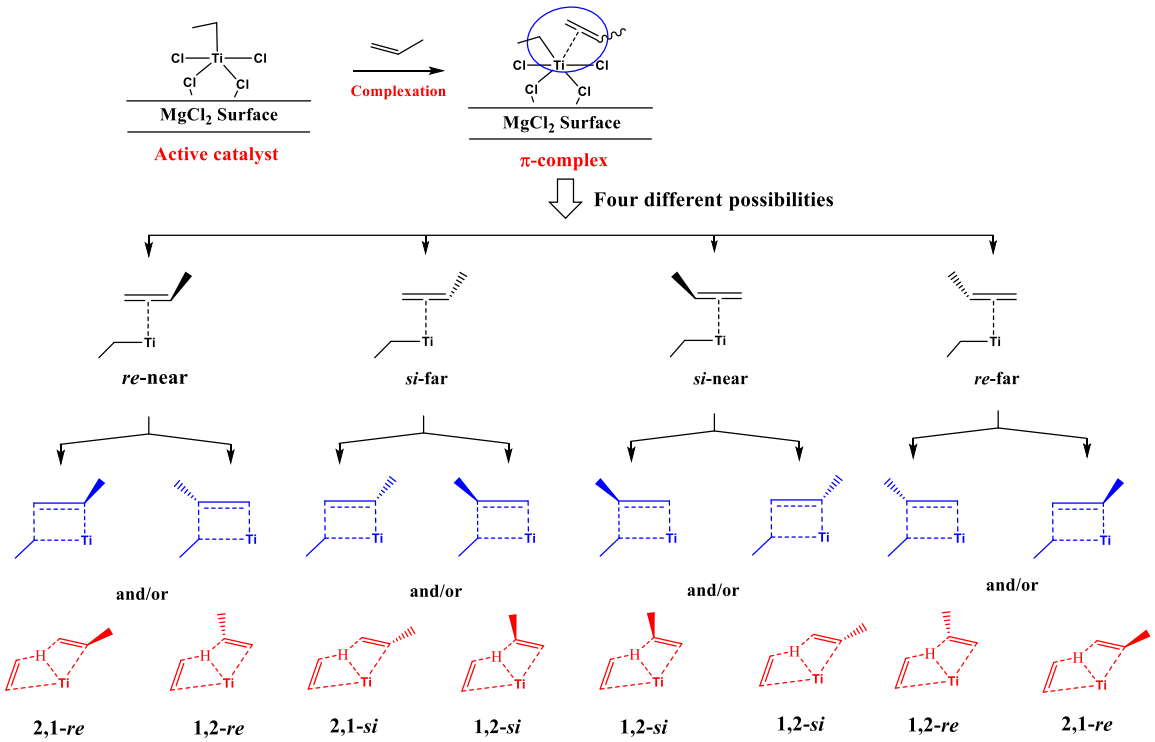

Scheme 1. Different p-complex, insertion and termination possibilities in propylene polymerization.

The stereoselective behaviour of mono- and bimetallic active sites have been considered in propylene polymerization. As mentioned above, four different p-complexations (where *re*-near and *re*-far, and *si*-far and *si*-near are energetically comparable) and insertion possibilities (1,2-*re*, 1,2-*si*, 2,1-*re*, and 2,1-*si*) are studied (Scheme 1). The insertion energy barriers for bimetallic active species (in the range of 26.9–29.6 kcal/mol) is higher compared to monometallic (6.7–13.3 kcal/mol). The reason is the same as mentioned in ethylene polymerization, stable octahedral titanium complex does not allow the olefin monomer to bound on the titanium centre easily. The optimized insertion transition state structures of all the possibilities are shown in Figure S11. These results suggest that the addition of aluminium in the bimetallic active site does not improve the regio- and stereoselective behaviour of titanium catalyst. Therefore, for further propylene polymerization study, only monometallic active site was considered.

Based on propylene polymerization mechanism discussed above, the effect of internal donors (IDs) on regio- and stereoselective of titanium catalyst are also studied. Table 5 shows the insertion and chain transfer to monomer energy barriers for propylene monomer with all the possibilities. The insertion energy barriers for Donor_3 is slightly lower with respect to other donor systems which is in the range of 8.0–9.7 kcal/mol. The ΔX values are in the range of 8.1–9.7 kcal/mol for the Donor_1, 5.4–9.7 kcal/mol for the Donor_2, 7.8–14.7 kcal/mol for the Donor_3, and 6.1–11.8 kcal/mol for the Donor_4 (Table 5). These results suggest that all the donor catalyst systems lead to higher molecular weight polymer in propylene polymerization. However, Donor_3 catalyst is producing slightly higher molecular weight polymer and showing more stereoselective behaviour compared to other donor catalyst systems. Figure 12 shows the more favourable energy barrier corresponding to the 1,2-*re* for Donor_1, 1,2-*re* for the Donor_2, 1,2-*si* for the Donor_3, and 2,1-*si* for the Donor_4. The difference between 1,2-insertion and 2,1-insertion ($\Delta G^{\ddagger}_{regio}$) suggests the regioselective nature of the Ti-catalyst, whereas enantioselective nature occurs due to differences in both the enantioselective (*re*/*si*) phases. For all the donor cases, the titanium catalyst is less regioselective because of less difference between 1,2 and 2,1 phases. However, a more enantioselective nature of Ti-catalyst was observed for all the donor catalyst systems (Figure 12).

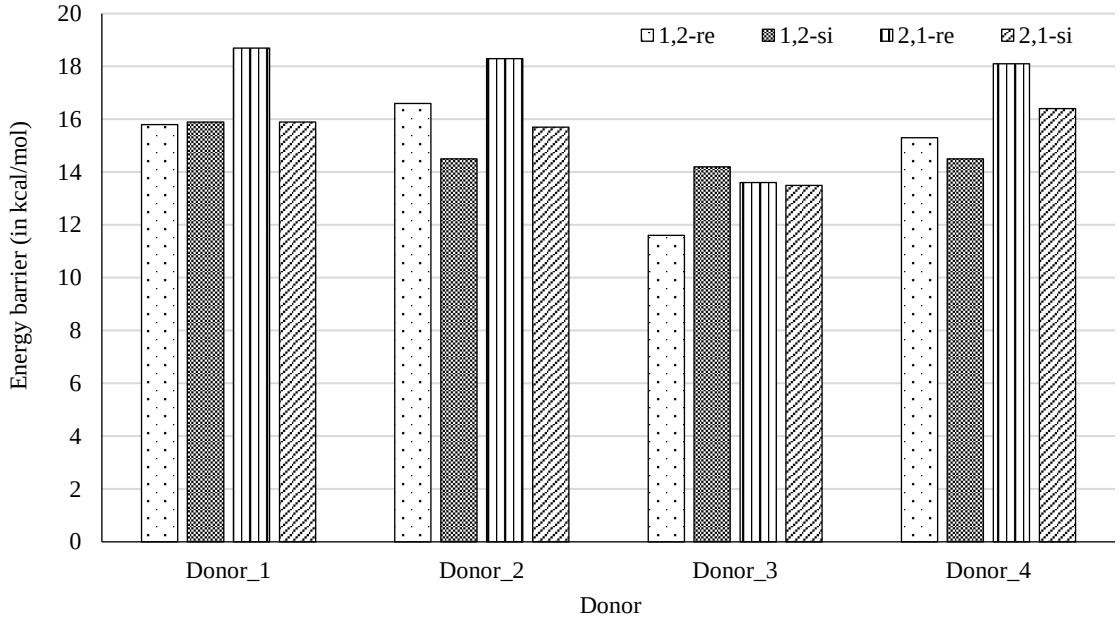

Figure 12. A bar graph for the comparative study of regio- and stereoselective behaviour of titanium catalysts using Donor_1, Donor_2, Donor_3, and Donor_4.

Table 5. Effect of IDs on propylene polymerization.

S.N.	Catalyst system	Energy barrier	ΔG (in kcal/mol)			
			1,2-re	***1,2-si***	***2,1-re***	***2,1-si***
1	Donor_1	Insertion (x)	15.8	17.1	17.5	15.9
		Termination (y)	20.4	26.8	26.8	24.5
		ΔX=(y)–(x)	4.6	9.7	9.3	8.6
2	Donor_2	Insertion (x)	11.6	14.2	13.6	13.5
		Termination (y)	17.9	19.6	23.3	19.8
		ΔX=(y)–(x)	6.3	5.4	9.7	6.3
3	Donor_3	Insertion (x)	9.7	8.0	9.2	9.3
		Termination (y)	17.5	19.8	23.9	22.2
		ΔX=(y)–(x)	7.8	11.8	14.7	12.9
4	Donor_4	Insertion (x)	16.8	16.8	18.3	15.1
		Termination (y)	22.9	25.7	24.5	26.9
		ΔX=(y)–(x)	6.1	8.9	13.2	11.8

The effect of alkoxysilane external donor on the propylene polymerization has been studied compared to the internal donor alone. For this study, Donor_1 and Donor_2 catalyst systems were considered. Table 6 shows that the addition of alkoxy silane increases the insertion and termination barriers; termination even more due to more constrained six-membered transition state. The reason is that the addition of an alkoxysilane donor on the $MgCl_2$ surface blocks some of the space of the titanium centre, which hinders the incoming monomer to approach on the titanium site. Therefore, overall, it increases the *DX* values which are in the range of 7.7–10.5 and 7.8–11.6 kcal/mol for the alkoxysilane containing Donor_1 and Donor_2 which is higher than the lone Donor_1 and Donor_2 donor, 8.1–9.7 and 5.4–9.7 kcal/mol, respectively (Table 6). These results suggest that adding alkoxysilane external donor in the Z-N system leads to the higher molecular weight polymer than the lone internal donor catalyst systems, which is equivalent to the experimental findings [73].

Table 6. Effect of alkoxysilane in propylene polymerization.

S.N.	Catalyst system		Energy barrier/Phase	ΔG (kcal/mol)			
	ID	ED		***1,2-re***	***1,2-si***	***2,1-re***	***2,1-si***
1	Donor_1	None	Insertion (x)	15.8	15.9	18.7	15.9
			Termination (y)	20.4	25.6	26.8	24.5
			ΔX=(y)–(x)	4.6	9.7	8.1	8.6
2	Donor_1	Alkoxysilane	Insertion (x)	16.6	14.5	18.3	15.7
			Termination (y)	24.3	25.0	26.1	25.2
			ΔX=(y)–(x)	7.7	10.5	7.8	9.5
3	Donor_2	None	Insertion (x)	11.6	14.2	13.6	13.5
			Termination (y)	17.9	19.6	23.3	19.8
			ΔX=(y)–(x)	6.3	5.4	9.7	6.3
4	Donor_2	Alkoxysilane	Insertion (x)	15.3	14.5	18.1	16.4
			Termination (y)	23.1	26.1	27.5	25.3
			ΔX=(y)–(x)	7.8	11.6	9.4	8.9

Moreover, alkoxysilane containing Donor_2 produced a higher molecular weight polymer compared to the alkoxysilane containing Donor_1, which further validates the experimental results [43, 44]. The insertion range for the propylene monomer is 3.8 and 3.6 kcal/mol for the alkoxysilane containing Donor_1 and Donor_2, which is almost same as lone Donor_1 and Donor_2 (2.9 and 2.6 kcal/mol). These differences explain the regio- and stereoselective nature of the titanium catalyst. Figure S12 shows the $\Delta G^{\ddagger}_{enantiomer}$ is higher for the 2,1-insertion than the 1,2-insertion for all the donor catalyst systems. For all the systems, the preferred path for the propylene monomer is 1,2-insertion. Among all, the alkoxysilane containing Donor_1 and Donor_2 catalyst systems are observed to be more stereoselective in nature for propylene polymerization compared to lone Donor_1 and Donor_2 systems.

CONCLUSION

The quantum chemical calculations have been carried out to study the role of carbonate- and ester-based electron donors in $MgCl_2$ supported Ziegler-Natta (Z-N) catalysis. Initially, the internal donors' (Donor_1, Donor_2, Donor_3 (carbonate-based), Donor_4 (ester–based), and DIBP) coordination to the $MgCl_2$ surface was investigated through mono-, chelate-, and bridge coordination. We observed that the bridge coordination mode was thermodynamically more favourable among the other coordination. Furthermore, in the case of Donor_3 (as a representative example), the phenyl ring (mainly responsible for the NCIs) was replaced by cyclohexane (Cy), methyl (Me) and biphenyl (Ph-Ph) groups for the donor coordination, which significantly influence the surface stabilization.

The effect of electron donors on the catalyst activation mechanism was studied in the presence/absence of an alkoxysilane external donor. The DFT calculations suggest that the presence of electron donors, (ID) and (ED), slightly slows the catalyst activation process. The reaction rate for the catalyst activation process has been observed in the following order: *wd*>ID>ED. In addition, a comparative study of bimetallic ($TiCl_2$-Et-Cl-$AlEt_2$), recently reported by Coperet *et al.* [69] and the monometallic ($TiCl_2$-Et) conventional active site was investigated for olefin polymerization. The quantum chemical calculations suggest that the bimetallic active site is less effective for the olefin polymerization than the conventional active site because of the stable octahedral titanium complex, which is not allowing the ethylene monomer to bound on the titanium centre easily.

The role of various electron donors (Donor_1, Donor_2, Donor_3, and Donor_4) on ethylene polymerization have been studied using the monometallic active site. It was observed that these donors lead to higher molecular weight polymer compared to conventional phthalate (DIBP) donor [74–77]. Moreover, to investigate the effect of different alkyl substituents on ethylene polymerization, a modification in Donor_3 was performed by replacing the phenyl with Cy, Me, and Ph-Ph. Some of

these alkyl substituents are enhancing the polymerization process, where NCIs played a vital role. Additionally, the effect of donors (ID and/or ED) on the regio- and stereoselective behaviour of the Ti-catalyst was also studied in propylene polymerization. These results suggest that the addition of alkoxysilane in the Z-N catalyst improves the molecular weight of the polymer and the stereoselectivity behaviour of Ti-catalyst in propylene polymerization. The alkoxysilane external donor sits beside the titanium centre on the $MgCl_2$ surface, and increasing the insertion and termination barriers; termination even more due to a more constrained transition state. Alkoxysilane increases the molecular weight of the polymer in Z-N which is validating the experimental findings [78–82]. Moreover, as observed in experimental study [43, 44] that the alkoxysilane containing Donor_2 produced a higher molecular weight polymer than the alkoxysilane containing Donor_1, which is also validated by DFT [83–90].

The hydrogen response for all the donor catalyst systems were also studied with respect to the DIBP and diether. It was observed that these donors have a better hydrogen response than the conventional DIBP and diether donor-based catalyst systems. Therefore, these chemical calculations provide interesting insights into the nature of active sites and olefin polymerization mechanism that would help the experimentalists to design a robust Z-N catalyst [91–100].

Supporting Information

Cartesian coordinates of all the intermediates and transition state structures are mentioned in the supporting information. Moreover, some of Figures are also composed in the article.

Data Availability

Data will be made available on request.

Acknowledgement

Authors would like to acknowledge the CSIR-National Chemical Laboratory (CSIR-NCL), Pune for providing the computational facility.

Conflicts of Interest

There are no conflicts to declare.

REFERENCES

1. Ziegler K. Wer ist's?— Karl Ziegler. Nachr Chem Tech. 1956 Jun;4(6):78–9. doi: https://doi.org/10.1002/nadc.19560040603.
2. Ziegler K, Holzkamp E, Breil H, Martin H. Das mülheimer normaldruck-polyäthylen-verfahren. Angew Chemie. 1955 Oct 7; 67(19–20): 541–7.
3. Natta G. Stereospecific macromolecules. J Polym Sci. 1955; 16: 143.
4. Natta G, Pino P, Corradini P, Danusso F, Mantica E, Mazzanti G, Moraglio G. Crystalline high polymers of α-olefins. J Am Chem Soc. 1955 Mar; 77(6): 1708–10.
5. Kashiwa N, Fujimura H, Tokuzumi Y. JP Patent, 1031698. 1968.
6. Kashiwa N. The discovery and progress of MgCl2-supported TiCl4 catalysts. J Polym Sci A: Polym Chem. 2004 Jan 1; 42(1): 1–8.
7. Luciani L, Kashiwa N, Barbè C, Toyota A. α-Olefin polymerization catalyst. Japanese Patent. 1977; 151.
8. Kumawat J, Gupta VK, Vanka K. Donor decomposition by Lewis acids in Ziegler–Natta catalyst systems: a computational investigation. Organometallics. 2014 Sep 8; 33(17): 4357–67.
9. Kumawat J, Gupta VK, Vanka K. Effect of donors on the activation mechanism in Ziegler–Natta catalysis: a computational study. ChemCatChem. 2016 May 20; 8(10): 1809–18.
10. Kumawat J, Kumar Gupta V, Vanka K. The nature of the active site in Ziegler–Natta olefin polymerization catalysis systems–A computational investigation. Eur J Inorg Chem. 2014 Oct; 2014(29): 5063–76.
11. Bahri-Laleh N, Correa A, Mehdipour-Ataei S, Arabi H, Haghighi MN, Zohuri G, Cavallo L. Moving up and down the titanium oxidation state in Ziegler− Natta catalysis. Macromolecules. 2011 Feb 22; 44(4): 778–83.

12. Cavallo L, Del Piero S, Ducéré JM, Fedele R, Melchior A, Morini G, Piemontesi F, Tolazzi M. Key interactions in heterogeneous Ziegler− Natta catalytic systems: Structure and energetics of TiCl4− Lewis base complexes. J Phys Chem C. 2007 Mar 22; 111(11): 4412–9.
13. Credendino R, Liguori D, Fan Z, Morini G, Cavallo L. Toward a unified model explaining heterogeneous Ziegler–Natta catalysis. ACS Catal. 2015 Sep 4; 5(9): 5431–5.
14. Correa A, Credendino R, Pater JT, Morini G, Cavallo L. Theoretical Investigation of Active Sites at the Corners of MgCl2 Crystallites in Supported Ziegler–Natta Catalysts. Macromolecules. 2012 May 8; 45(9): 3695–701.
15. Correa A, Piemontesi F, Morini G, Cavallo L. Key elements in the structure and function relationship of the MgCl2/TiCl4/Lewis base Ziegler− Natta catalytic system. Macromolecules. 2007 Dec 11; 40(25): 9181–9.
16. Credendino R, Liguori D, Morini G, Cavallo L. Investigating phthalate and 1, 3-diether coverage and dynamics on the (104) and (110) surfaces of MgCl2-supported Ziegler–Natta catalysts. J Phys Chem C. 2014 Apr 17; 118(15): 8050–8.
17. Vipin Raj K, Kumawat J, Dhamaniya S, Subaramanian M, Balaraman E, Kumar Gupta V, Vanka K, Grubbs RH. Insights into the Nature of Self-Extinguishing External Donors for Ziegler-Natta Catalysis: A Combined Experimental and DFT Study. ChemCatChem. 2021 Jan 20; 13(2): 674–81.
18. Kumawat J, Gupta VK, Vanka K. Role of the (104) MgCl2 lateral cut in Ziegler–Natta catalysis: a computational investigation. J Phys Chem C. 2018 Jan 11; 122(1): 285–96.
19. Zorve P, Linnolahti M. Catalytic reactions on magnesium dichloride clusters saturated by titanium tetrachloride. Mol Catal. 2021 Jan 1; 499: 111314.
20. Bahri-Laleh N, Hanifpour A, Mirmohammadi SA, Poater A, Nekoomanesh-Haghighi M, Talarico G, Cavallo L. Computational modeling of heterogeneous Ziegler-Natta catalysts for olefins polymerization. Prog Polym Sci. 2018 Sep 1; 84: 89–114.
21. Bazhenov AS, Denifl P, Leinonen T, Pakkanen A, Linnolahti M, Pakkanen TA. Modeling coadsorption of titanium tetrachloride and bidentate electron donors on magnesium dichloride support surfaces. J Phys Chem C. 2014 Dec 4; 118(48): 27878–83.
22. Wondimagegn T, Ziegler T. The role of external alkoxysilane donors on stereoselectivity and molecular weight in MgCl2-supported Ziegler–Natta propylene polymerization: a density functional theory study. J Phys Chem C. 2012 Jan 12; 116(1): 1027–33.
23. Seth M, Margl PM, Ziegler T. A density functional embedded cluster study of proposed active sites in heterogeneous Ziegler− Natta catalysts. Macromolecules. 2002 Sep 24; 35(20): 7815–29.
24. Seth M, Ziegler T. Theoretical Study of the Copolymerization of Ethylene and Propylene by a Heterogeneous Ziegler− Natta Catalyst. Macromolecules. 2004 Nov 30; 37(24): 9191–200.
25. Seth M, Ziegler T. Polymerization Properties of a heterogeneous Ziegler− Natta catalyst modified by a base: A theoretical study. Macromolecules. 2003 Aug 26; 36(17): 6613–23.
26. Potapov AG, Bukatov GD, Zakharov VA. DRIFTS study of the interaction of the AlEt3 cocatalyst with the internal donor ethyl benzoate in supported Ziegler–Natta catalysts. J Mol Catal A: Chem. 2009 Mar 18; 301(1–2): 18–23.
27. Busico V, Corradini P, De Martino L, Proto A, Savino V, Albizzati E. Polymerization of propene in the presence of MgCl2-supported Ziegler-Natta catalysts, 1. The role of ethyl benzoate as “internal” and “external” base. Die Makromolekulare Chemie: Macromol Chem Phys. 1985 Jun; 186(6): 1279–88.
28. da Silveira JM, Chikuma H, Takasao G, Wada T, Chammingkwan P, Taniike T. Deciphering the Role of Internal Donors in Shaping Heterogeneous Ziegler–Natta Catalysts Based on Nonempirical Structural Determination. ACS Catal. 2024 Jan 30; 14(4): 2300–12.
29. Potapov AG, Bukatov GD, Zakharov VA. DRIFTS study of the interaction of the internal donor in TiCl4/di-n-butyl phthalate/MgCl2 catalysts with AlEt3 cocatalyst. J Mol Catal A: Chem. 2010 Feb 1; 316(1–2): 95–9.
30. Song BG, Ihm SK. The role of two different internal donors (phthalate and 1, 3-diether) on the formation of surface structure in MgCl2-supported Ziegler–Natta catalysts and their catalytic performance of propylene polymerization. J Appl Polym Sci. 2014 Aug 5; 131(15): 40536.

31. Blaakmeer EM, Antinucci G, van Eck ER, Kentgens AP. Probing interactions between electron donors and the support in MgCl2-supported Ziegler–Natta catalysts. J Phys Chem C. 2018 Jul 17; 122(31): 17865–81.
32. Breuza E, Antinucci G, Budzelaar PH, Busico V, Correa A, Ehm C. MgCl2-Supported Ziegler–Natta catalysts: a DFT-D "flexible-cluster" approach to internal donor adducts. J Phys Chem C. 2018 Apr 4; 122(16): 9046–53.
33. Credendino R, Pater JT, Correa A, Morini G, Cavallo L. Thermodynamics of formation of uncovered and dimethyl ether-covered MgCl2 crystallites. Consequences in the structure of Ziegler–Natta heterogeneous catalysts. J Phys Chem C. 2011 Jul 14; 115(27): 13322–8.
34. Chadwick JC, Morini G, Albizzati E, Balbontin G, Mingozzi I, Cristofori A, Sudmeijer O, Van Kessel GM. Aspects of hydrogen activation in propene polymerization using MgCl2/TiCl4/diether catalysts. Macromol Chem Phys. 1996 Aug; 197(8): 2501–10.
35. Blaakmeer EM, Antinucci G, Correa A, Busico V, van Eck ER, Kentgens AP. Structural characterization of electron donors in Ziegler–Natta catalysts. J Phys Chem C. 2018 Feb 21; 122(10): 5525–36.
36. Wen X, Ji M, Yi Q, Niu H, Dong JY. Magnesium chloride supported Ziegler-Natta catalysts containing succinate internal electron donors for the polymerization of propylene. J Appl Polym Sci. 2010 Nov 5; 118(3): 1853–8.
37. Matsunaga K, Hashida H, Tsutsui T, Yamamoto K, Shibahara A, Shinozaki T. US Patent 7,888,438. 2011.
38. Liang P, Li W, Chen Y, Dong C, Zhou Q, Feng Y, Chen M, Dai J, Ren C, Jiang B, Wang J. Revealing the dynamic behaviors of tetrahydrofuran for tailoring the active species of Ziegler–Natta catalysts. ACS Catal. 2021 Mar 26; 11(8): 4411–21.
39. Grau E, Lesage A, Norsic S, Copéret C, Monteil V, Sautet P. Tetrahydrofuran in TiCl4/THF/MgCl2: a non-innocent ligand for supported ziegler–natta polymerization catalysts. ACS Catal. 2013 Jan 4; 3(1): 52–6.
40. Zhao A, Liu J, Zhou R, Yang X, He A. A DFT study on the role of alkoxysilanes in the polymerization of isoprene over Ziegler-Natta catalyst. Comput Theor Chem. 2024 Jul 1; 1237: 114661.
41. Khatri V, Sahoo U, Kaur S, Rani R, Singh G, Kapur GS, Kashyap HK. Control of Ziegler–Natta catalyst activity by the structural design of alkoxysilane-based external donors. New J Chem. 2020; 44(17): 6845–52.
42. Chadwick JC, Miedema A, Sudmeijer O. Hydrogen activation in propene polymerization with MgCl2-supported Ziegler-Natta catalysts: the effect of the external donor. Macromol Chem Phys. 1994 Jan; 195(1): 167–72.
43. Chadwick JC, Morini G, Balbontin G, Camurati I, Heere JJ, Mingozzi I, Testoni F. Effects of Internal and External Donors on the Regio-and Stereoselectivity of Active Species in MgCl2-supported catalysts for propene polymerization. Macromol Chem Phys. 2001 Jun 1; 202(10): 1995–2002.
44. Vittoria A, Meppelder A, Friederichs N, Busico V, Cipullo R. Ziegler–Natta catalysts: Regioselectivity and "hydrogen response". ACS Catal. 2019 Dec 2; 10(1): 644–51.
45. Zhang J, Nan F, Yu H, Zhang S, Xia X, Huang Q, Yi J, Li H, Zhao Z. Direct Preparation of Transparent Isotactic Polypropylene with Supported Ziegler–Natta Catalysts Containing Novel Eco-friendly Internal Electron Donors. Ind Eng Chem Res. 2020 Apr 16; 59(19): 8995–9003.
46. Coalter III JN, Leung TW, Tao T, Gao K. Dow Global Techn. Inc., US 8633126. 2010.
47. Matta A, Chammingkwan P, Singh BK, Terano M, Kaneko T, Taniike T. Truxillic and truxinic acid-based, bio-derived diesters as potent internal donor in Ziegler-Natta catalyst for propylene polymerization. Appl Catal A: Gen. 2018 Mar 25; 554: 80–7.
48. Kumawat J, Trivedi P, Gupta VK. Role of a multidentate carbonate donor in MgCl2-supported Ziegler–Natta olefin polymerization catalysis: An experimental and computational approach. J Phys Chem C. 2019 Sep 17; 123(40): 24501–10.
49. Nissinen VH, Linnolahti M, Bazhenov AS, Pakkanen TT, Pakkanen TA, Denifl P, Leinonen T, Jayaratne K, Pakkanen A. Polyethylenimines: multidentate electron donors for Ziegler–Natta catalysts. J Phys Chem C. 2017 Oct 26; 121(42): 23413–21.

50. Ratanasak M, Hasegawa JY, Parasuk V. Roles of salicylate donors in enhancement of productivity and isotacticity of Ziegler–Natta catalyzed propylene polymerization. Polymers. 2020 Apr 10; 12(4): 883.
51. Dangat Y, Popli S, Sunoj RB. Unraveling the importance of noncovalent interactions in asymmetric hydroformylation reactions. J Am Chem Soc. 2020 Sep 16; 142(40): 17079–92.
52. Reddi Y, Tsai CC, Avila CM, Toste FD, Sunoj RB. Harnessing noncovalent interactions in dual-catalytic enantioselective Heck–Matsuda arylation. J Am Chem Soc. 2018 Dec 18; 141(2): 998–1009.
53. Bhaskararao B, Sunoj RB. Two chiral catalysts in action: insights into cooperativity and stereoselectivity in proline and cinchona-thiourea dual organocatalysis. Chem Sci. 2018; 9(46): 8738–47.
54. Straker RN, Peng Q, Mekareeya A, Paton RS, Anderson EA. Computational ligand design in enantio-and diastereoselective ynamide [5+ 2] cycloisomerization. Nat Commun. 2016 Jan 5; 7(1): 10109.
55. Stukalov DV, Zakharov VA. Active Site Formation in MgCl2− Supported Ziegler− Natta Catalysts. A Density Functional Theory Study. J Phys Chem C. 2009 Dec 24; 113(51): 21376–82.
56. Singh G, Kaur S, Makwana U, Patankar RB, Gupta VK. Influence of internal donors on the performance and structure of MgCl2 supported titanium catalysts for propylene polymerization. Macromol Chem Phys. 2009 Jan 2; 210(1): 69–76.
57. Makwana UC, Gupta V. Trans-1, 4-polybutadiene: Influences of Lewis bases on polymerization of butadiene with supported titanium catalyst systems. J Macromol Sci A. 2021 Nov 1; 58(11): 820–34.
58. Ahlrichs R, Bär M, Häser M, Horn H, Kölmel C. Electronic structure calculations on workstation computers: The program system turbomole. Chem Phys Lett. 1989 Oct 13; 162(3): 165–9.
59. Becke AD. Density-functional exchange-energy approximation with correct asymptotic behavior. Phys Rev A. 1988 Sep 1; 38(6): 3098–3100.
60. Perdew JP. Density-functional approximation for the correlation energy of the inhomogeneous electron gas. Phys Rev B Condens Matter. 1986 Jun 15; 33(12): 8822–8824.
61. Bahri-Laleh N, Credendino R, Cavallo L. The intriguing modeling of cis–trans selectivity in ruthenium-catalyzed olefin metathesis. Beilstein J Org Chem. 2011 Jan 13;7(1):40–5. doi: https://doi.org/10.3762/bjoc.7.7.
62. Zhao Y, Truhlar DG. The M06 suite of density functionals for main group thermochemistry, thermochemical kinetics, noncovalent interactions, excited states, and transition elements: two new functionals and systematic testing of four M06-class functionals and 12 other functionals. Theor Chem Acc. 2008 May; 120(1): 215–41.
63. Frisch MJ, Trucks GW, Schlegel HB, Scuseria GE, Robb MA, Cheeseman JR, Scalmani G, Barone V, Petersson GA, Nakatsuji H, Li X. Gaussian 16, revision a. 03, gaussian, inc., wallingford ct. Gaussian16 (Revision A. 03). 2016.
64. Eichkorn K, Treutler O, Öhm H, Häser M, Ahlrichs R. Auxiliary basis sets to approximate Coulomb potentials. Chem Phys Lett. 1995 Jun 30; 240(4): 283–90.
65. Sierka M, Hogekamp A, Ahlrichs R. Fast evaluation of the Coulomb potential for electron densities using multipole accelerated resolution of identity approximation. J Chem Phys. 2003 May 22; 118(20): 9136–48.
66. Fukui K. The path of chemical reactions-the IRC approach. Acc Chem Res. 1981 Dec 1; 14(12): 363–8.
67. Linnolahti M, Pakkanen TA, Bazhenov AS, Denifl P, Leinonen T, Pakkanen A. Alkylation of titanium tetrachloride on magnesium dichloride in the presence of Lewis bases. J Catal. 2017 Sep 1; 353: 89–98.
68. Zorve P, Linnolahti M. Adsorption of titanium tetrachloride on magnesium dichloride clusters. ACS omega. 2018 Aug 24; 3(8): 9921–8.
69. Ashuiev A, Humbert M, Norsic S, Blahut J, Gajan D, Searles K, Klose D, Lesage A, Pintacuda G, Raynaud J, Monteil V. Spectroscopic signature and structure of the active sites in Ziegler–Natta polymerization catalysts revealed by electron paramagnetic resonance. J Am Chem Soc. 2021 Jun 25; 143(26): 9791–7.

70. Arlman EJ, Cossee P. Ziegler-Natta catalysis III. Stereospecific polymerization of propene with the catalyst system TiCl3 AlEt3. J Catal. 1964 Feb 1; 3(1): 99–104.
71. Kissin YV, Rishina LA. Hydrogen effects in propylene polymerization reactions with titanium-based Ziegler–Natta catalysts. I. Chemical mechanism of catalyst activation. J Polym Sci A: Polym Chem. 2002 May 1; 40(9): 1353–65.
72. Kissin YV, Rishina LA, Vizen EI. Hydrogen effects in propylene polymerization reactions with titanium-based Ziegler–Natta catalysts. II. Mechanism of the chain-transfer reaction. J Polym Sci A: Polym Chem. 2002 Jun 1; 40(11): 1899–911.
73. Corradini P, Guerra G, Cavallo L. Do new century catalysts unravel the mechanism of stereocontrol of old Ziegler− Natta catalysts? Acc Chem Res. 2004 Apr 20; 37(4): 231–41.
74. Sacchi MC, Forlini F, Tritto I, Mendichi R, Zannoni G, Noristi L. Activation effect of alkoxysilanes as external donors in magnesium chloride-supported Ziegler-Natta catalysts. Macromolecules. 1992 Oct; 25(22): 5914–8.
75. Sacchi MC, Tritto I, Shan C, Mendichi R, Noristi L. Role of the pair of internal and external donors in magnesium chloride-supported Ziegler-Natta catalysts. Macromolecules. 1991 Dec; 24(26): 6823–6.
76. Weng Y, Jiang B, Fu Z, Fan Z. Mechanism of internal and external electron donor effects on propylene polymerization with MgCl2-supported Z iegler–N atta catalyst: New evidences based on active center counting. J Appl Polym Sci. 2018 Aug 20; 135(32): 46605.
77. Niyomthai T, Jongsomjit B, Praserthdam P. Investigation of Alkoxysilanes in the Presence of Hydrogen with Ziegler-Natta Catalysts in Ethylene Polymerization. Eng J. 2017 Dec 29; 21(7): 171–80.
78. Brambilla L, Zerbi G, Piemontesi F, Nascetti S, Morini G. Structure of Donor Molecule 9, 9-Bis (Methoxymethyl)-Fluorene in Ziegler-Natta Catalyst by Infrared Spectroscopy and Quantum Chemical Calculation. J Phys Chem C. 2010 Jul 8; 114(26): 11475–84.
79. Brant P, Speca AN. Electron spin resonance, titanium oxidation state, and ethylene polymerization studies of a model supported Ziegler-Natta catalyst. Spectroscopic detection of titanium tetrachloride. Macromolecules. 1987 Nov; 20(11): 2740–4.
80. Busico V, Cipullo R, Monaco G, Vacatello M, Segre AL. Full assignment of the 13C NMR spectra of regioregular polypropylenes: Methyl and methylene region. Macromolecules. 1997 Oct 6; 30(20): 6251–63.
81. Kumawat J, Gupta VK. In silico approaches for olefin polymerization using transition metal catalyst systems. In: *In silico* Approaches to Macromolecular Chemistry. Elsevier; 2023 Jan 1; 313–348.
82. Niu Q, He A, Si C, Liu G, Xiao M, Chen G, Jin M. Influence of titanium loading of TiCl4/MgCl2 Ziegler-Natta catalyst on Trans-1, 4 polymerization of isoprene. Polymer. 2024 Jul 24; 307: 127317.
83. Trivedi PM, Gupta VK. Progress in MgCl2 supported Ziegler-Natta catalyzed polyolefin products and applications. J Polym Res. 2021 Feb; 28(2): 45.
84. Kumawat J, Gupta VK. Fundamental aspects of heterogeneous Ziegler–Natta olefin polymerization catalysis: An experimental and computational overview. Polym Chem. 2020; 11(38): 6107–28.
85. Koshevoy EI, Mikenas TB, Zakharov VA, Shubin AA, Barabanov AA. Electron paramagnetic resonance study of the interaction of surface titanium species with AlR3 cocatalyst in supported Ziegler–Natta catalysts with a low titanium content. J Phys Chem C. 2016 Jan 21; 120(2): 1121–9.
86. Bazvand R, Bahri-Laleh N, Nekoomanesh M, Abedini H. Highly efficient FeCl3 doped Mg (OEt) 2/TiCl4-based Ziegler–Natta catalysts for ethylene polymerization. Des Monomers Polym. 2015 Oct 3; 18(7): 599–610.
87. Panchenko VN, Goryachev AN, Vorontsova LV, Paukshtis EA, Zakharov VA. Basicity of Stereoregulating Electron-Donor Compounds in Ziegler–Natta Catalysts: A Study by Infrared Spectroscopy and Chemical Exchange Reactions. J Phys Chem C. 2014 Dec 11; 118(49): 28572–9.
88. Abazari M, Jamjah R, Bahri-Laleh N, Hanifpour A. Synthesis and evaluation of a new three-metallic high-performance Ziegler–Natta catalyst for ethylene polymerization: experimental and computational studies. Polym Bull. 2022 Sep; 79(9): 7265–80.
89. Trivedi PM, Gocher CP, Balachandran V, Gupta VK. Insight of polypropylene synthesis with high performance multidentate internal donor catalyst system. J Appl Polym Sci. 2023 Mar 15; 140(11): e53609.

90. Thomas ME, Thomas J, Thomas S, Kornweitz H, editors. In-Silico Approaches to Macromolecular Chemistry. Elsevier; 2023 Feb 28; 313.
91. Shen XR, Fu ZS, Hu J, Wang Q, Fan ZQ. Mechanism of propylene polymerization with MgCl2-supported Ziegler–Natta catalysts based on counting of active centers: The role of external electron donor. J Phys Chem C. 2013 Jul 25; 117(29): 15174–82.
92. Neel AJ, Hilton MJ, Sigman MS, Toste FD. Exploiting non-covalent π interactions for catalyst design. Nature. 2017 Mar 30; 543(7647): 637–46.
93. Wagner JP, Schreiner PR. London dispersion in molecular chemistry—reconsidering steric effects. Angew Chem Int Ed. 2015 Oct 12; 54(42): 12274–96.
94. Yakimov A, Xu J, Searles K, Liao WC, Antinucci G, Friederichs N, Busico V, Copéret C. DNP-SENS formulation protocols to study surface sites in Ziegler–Natta catalyst MgCl2 supports modified with internal donors. J Phys Chem C. 2021 Jul 20; 125(29): 15994–6003.
95. Cossee P. Ziegler-Natta catalysis I. Mechanism of polymerization of α-olefins with Ziegler-Natta catalysts. J Catal. 1964 Feb 1; 3(1): 80–8.
96. Talarico G, Budzelaar PH. Variability of chain transfer to monomer step in olefin polymerization. Organometallics. 2008 Aug 25; 27(16): 4098–107.
97. Talarico G, Budzelaar PH. A second transition state for chain transfer to monomer in olefin polymerization promoted by group 4 metal catalysts. J Am Chem Soc. 2006 Apr 12; 128(14): 4524–5.
98. Talarico G, Blok AN, Woo TK, Cavallo L. Comparison of ab initio and DFT methods for studying chain propagation and chain termination processes with group 4 polymerization catalysts. 1. The ansa-bis (cyclopentadienyl) zirconium catalyst. Organometallics. 2002 Nov 11; 21(23): 4939–49.
99. Chadwick JC, Van Der Burgt FP, Rastogi S, Busico V, Cipullo R, Talarico G, Heere JJ. Influence of Ziegler− Natta catalyst regioselectivity on polypropylene molecular weight distribution and rheological and crystallization behavior. Macromolecules. 2004 Dec 28; 37(26): 9722–7.
100. Busico V, Chadwick JC, Cipullo R, Ronca S, Talarico G. Propene/ethene-[1-13c] copolymerization as a tool for investigating catalyst regioselectivity. MgCl2/internal donor/TiCl4− external donor/AlR3 systems. Macromolecules. 2004 Oct 5; 37(20): 7437–43.

SUPPLEMENTARY

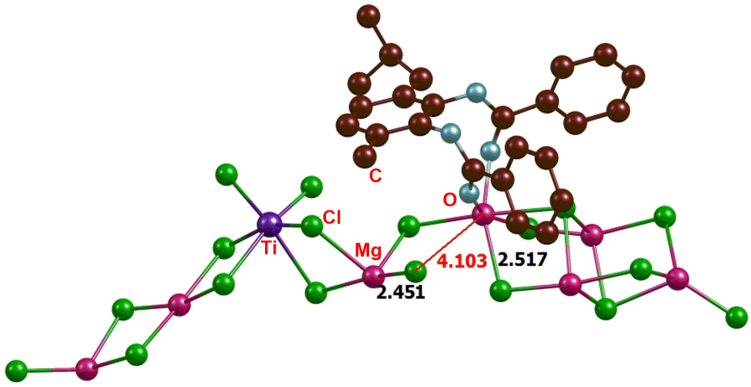

Figure S1. Optimized structure for Donor_4 coordinated to the $MgCl_2$ surface through chelate fashion; all the $MgCl_2$ layers and hydrogen atoms are not shown for the clarity.

Donor Displacement Study

A bar diagram for the relative thermodynamic values (DG) for the Ti-Cl bond cleavage and donor displacement are shown in Figure S4. These results suggest that the Ti-Cl bond cleavage is thermodynamically more favourable in comparison to the donor displacement in the presence of $AlEt_3$ moiety. As shown in Figure S4, the thermodynamic values are 19.1 and 16.7 kcal/mol for the Ti-Cl bond cleavage, and 34.5 and 30.3 kcal/mol for the donor displacement for Donor_1 and Donor_2 cases,

respectively. The reason is that the Donor_1 and Donor_2 bound to the $MgCl_2$ surface through two (C=O) oxygen atoms in a bridge coordination fashion. Therefore, it is more difficult to displace from the $MgCl_2$ surface in comparison to single Ti-Cl bond cleavage with the help of $AlEt_3$ moiety. The same results were also observed with alkoxy silane external donor (ED) system (Figure S4). However, ED enhances the Ti-Cl bond cleavage and donor (ID) displacement process due to more electronic rich system.

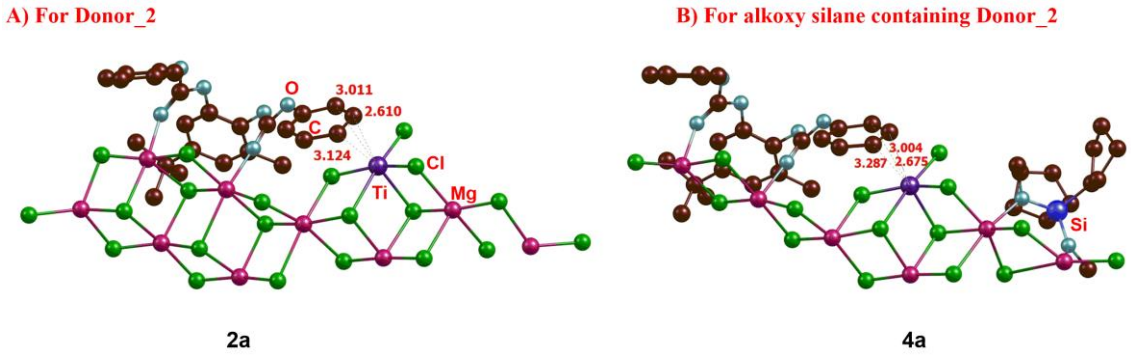

Figure S2. Optimized structure for the catalyst activation mechanism step where the NCIs of Donor_2 to the vacant titanium centre is shown in absence (**2a**) and presence of alkoxy silane (**4a**); all the $MgCl_2$ layers and hydrogen atoms are not shown for the clarity.

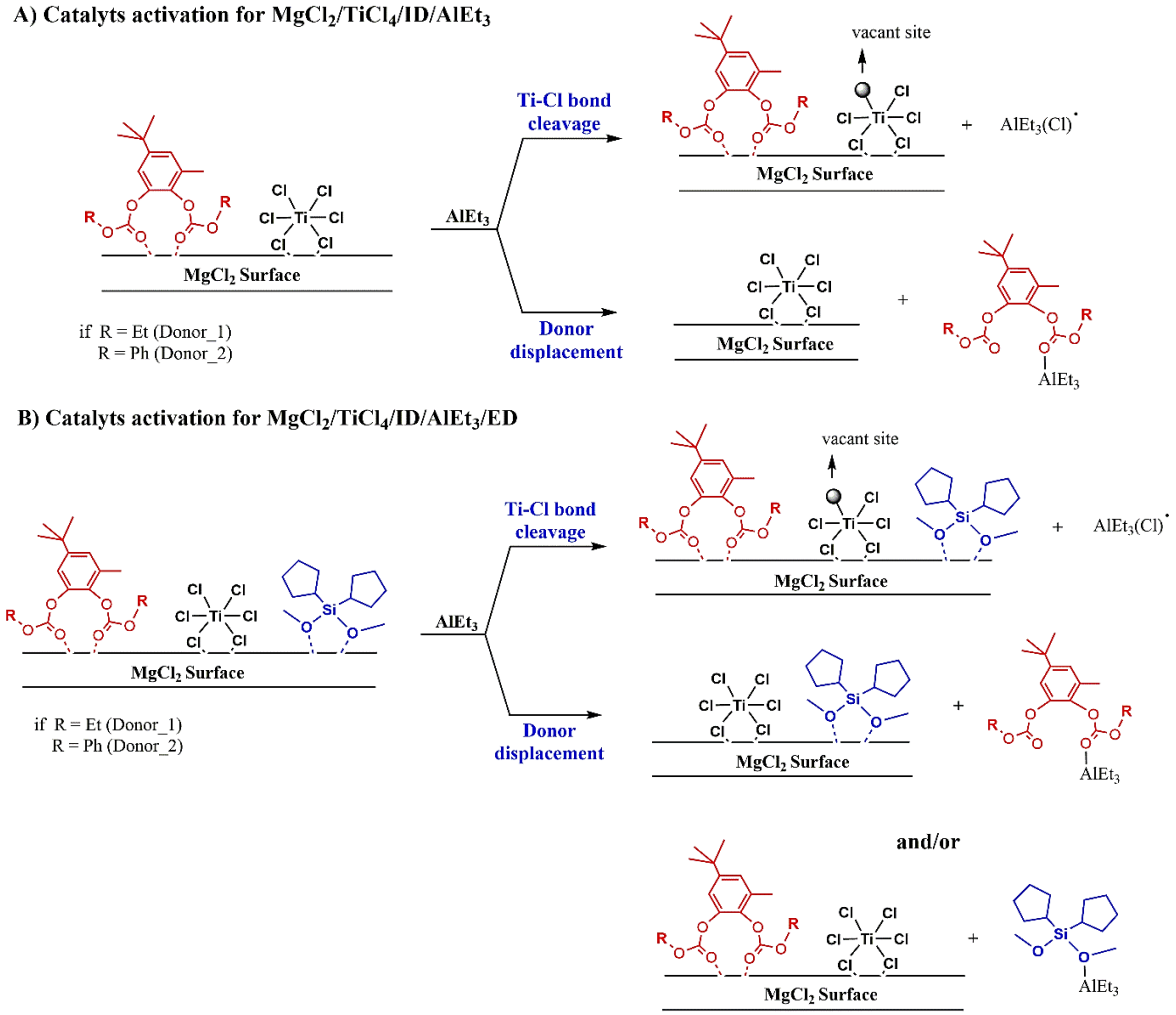

Figure S3. The Ti-Cl bond cleavage and donor displacement possibilities with (A) $MgCl_2$/$TiCl_4$/ID/$AlEt_3$ and (B) $MgCl_2$/$TiCl_4$/ID/$AlEt_3$/ED systems.

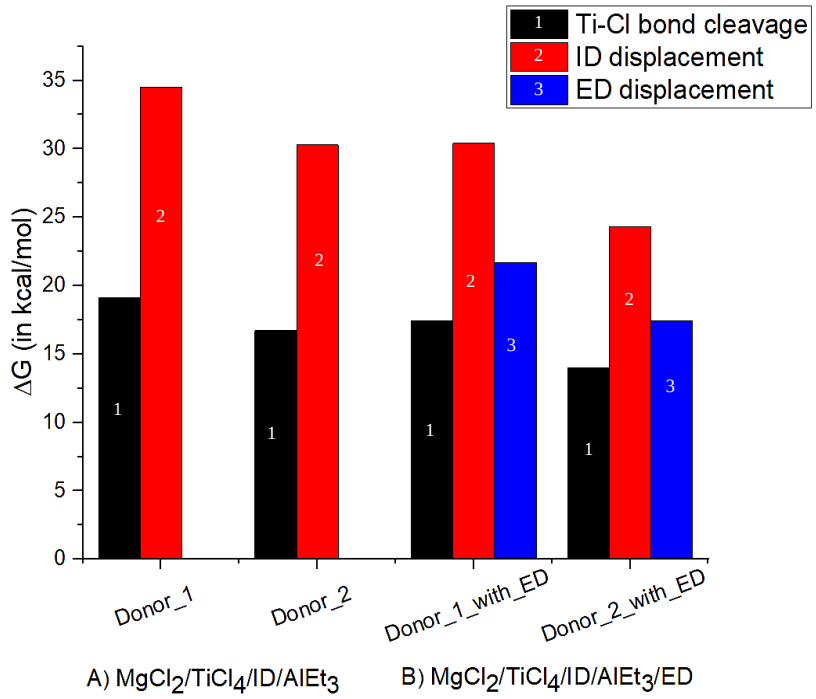

Figure S4. A bar graph for the comparative study between Ti-Cl bond cleavage and donor displacement (ID and ED).

Electronic and Steric Effect on Donor_3 for Ethylene Polymerization

Based on the ethylene polymerization mechanism for donors outlined in Figure 12, we also examined the effect of different substituents (cyclohexyl (Cy), methyl (Me) and biphenyl (Ph-Ph)) on propylene polymerization. Here, Donor_3 catalyst system is used as a representative example. Table S2 compiles all the steps for these substituted donor catalyst systems.

The insertion and termination barriers for the phenyl and biphenyl are lower compared to the cyclohexane and methyl due to NCI interactions with is helping in stabilising the transition state (Figures S7 and S8). However, phenyl and cyclohexane leads to higher molecular weight polymer with respect to methyl and biphenyl.

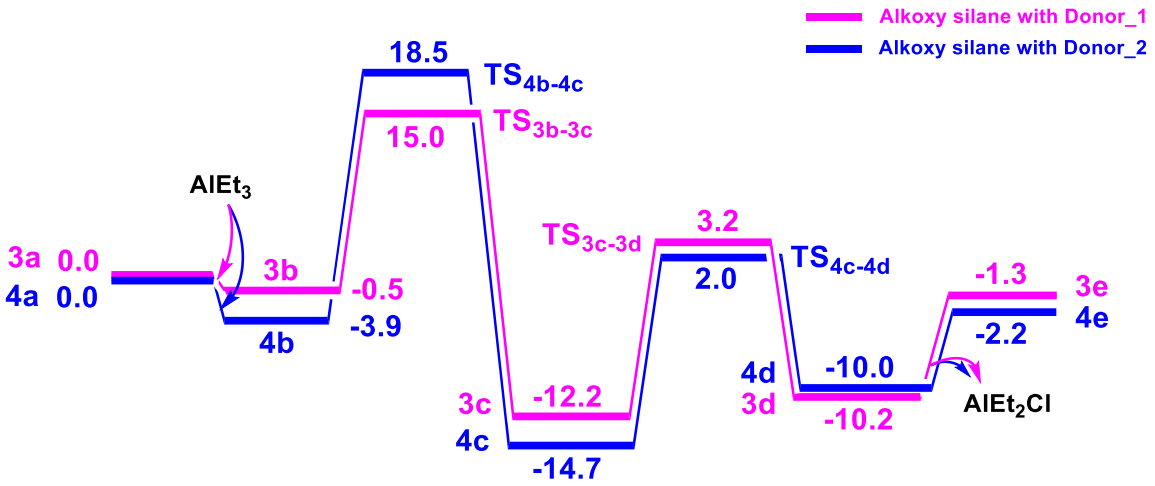

Figure S5. The free energy profile for the comparative study between alkoxy silane containing Donor_1 and the Donor_2 cases for the transalkylation step.

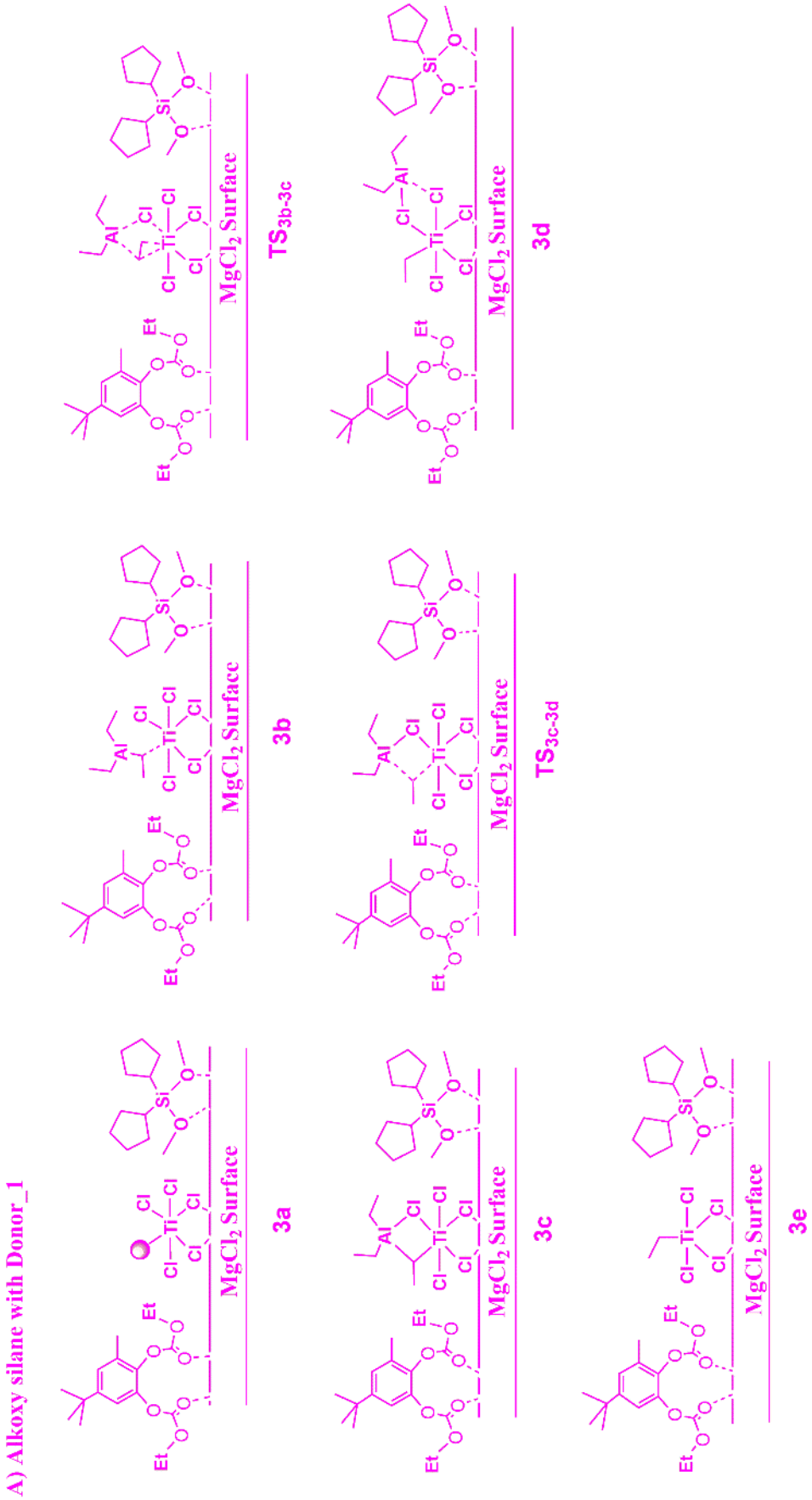

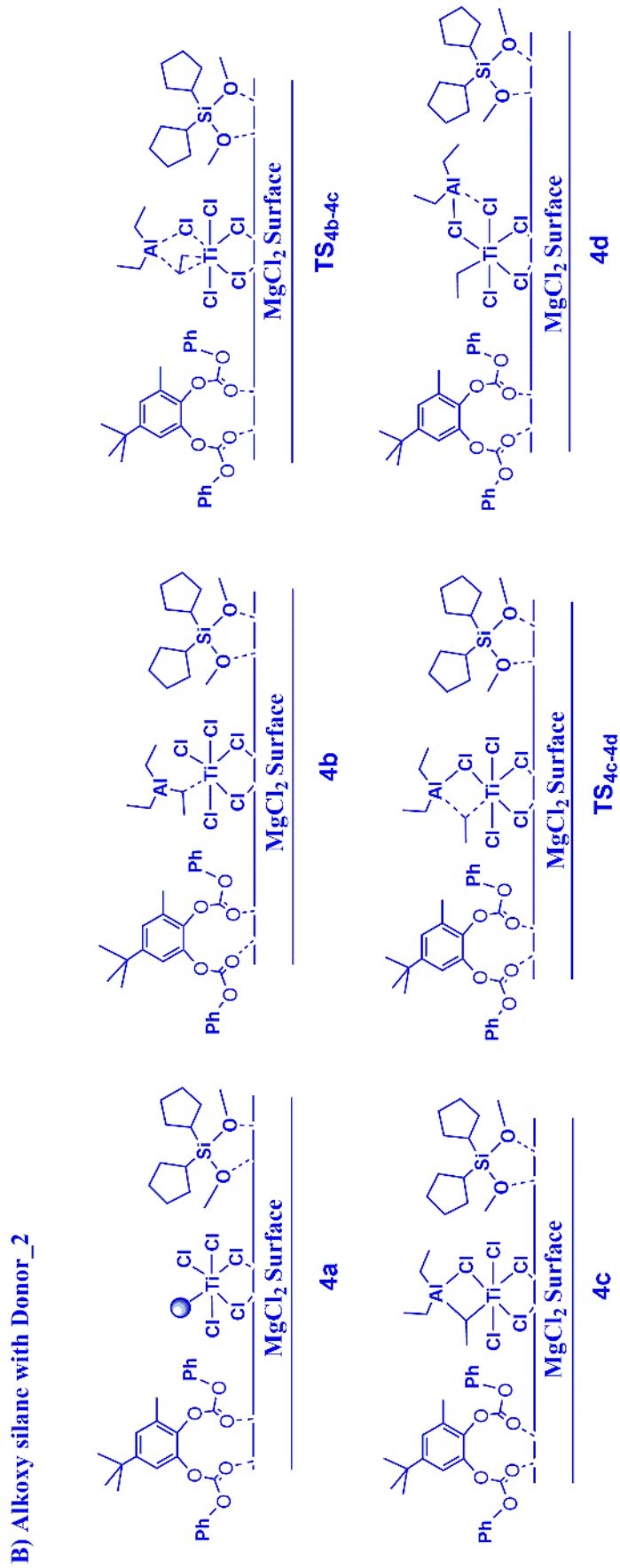

Figure S6. (a and b) Different intermediate and transition state structures that are indicated in Figure S5.

Table S1. A comparative study on catalyst activation mechanism using different donor catalyst systems.

Donor catalyst system x=1', 1, 2, 3 and 4			DG values (kcal/mol)							
	ID	ED	xa	xb	TS_{xb-xc}	Barrier	xc	TS_{xc-xd}	xd	xe
1'	None	None	0.0	0.2	12.9	**12.9**	–13.9	–0.7	–15.5	–4.6
1	Donor_1	None	0.0	2.3	15.9	**15.9**	–11.5	–2.5	–8.7	–5.6
2	Donor_2	None	0.0	–0.8	18.6	**19.4**	–6.9	–2.7	–13.4	2.2
3	Donor_1	alkoxysilane	0.0	–0.5	15.0	**15.5**	–12.2	3.2	–10.2	–1.3
4	Donor_2	alkoxysilane	0.0	–3.9	18.5	**22.4**	–14.7	2.0	–10.0	–2.2

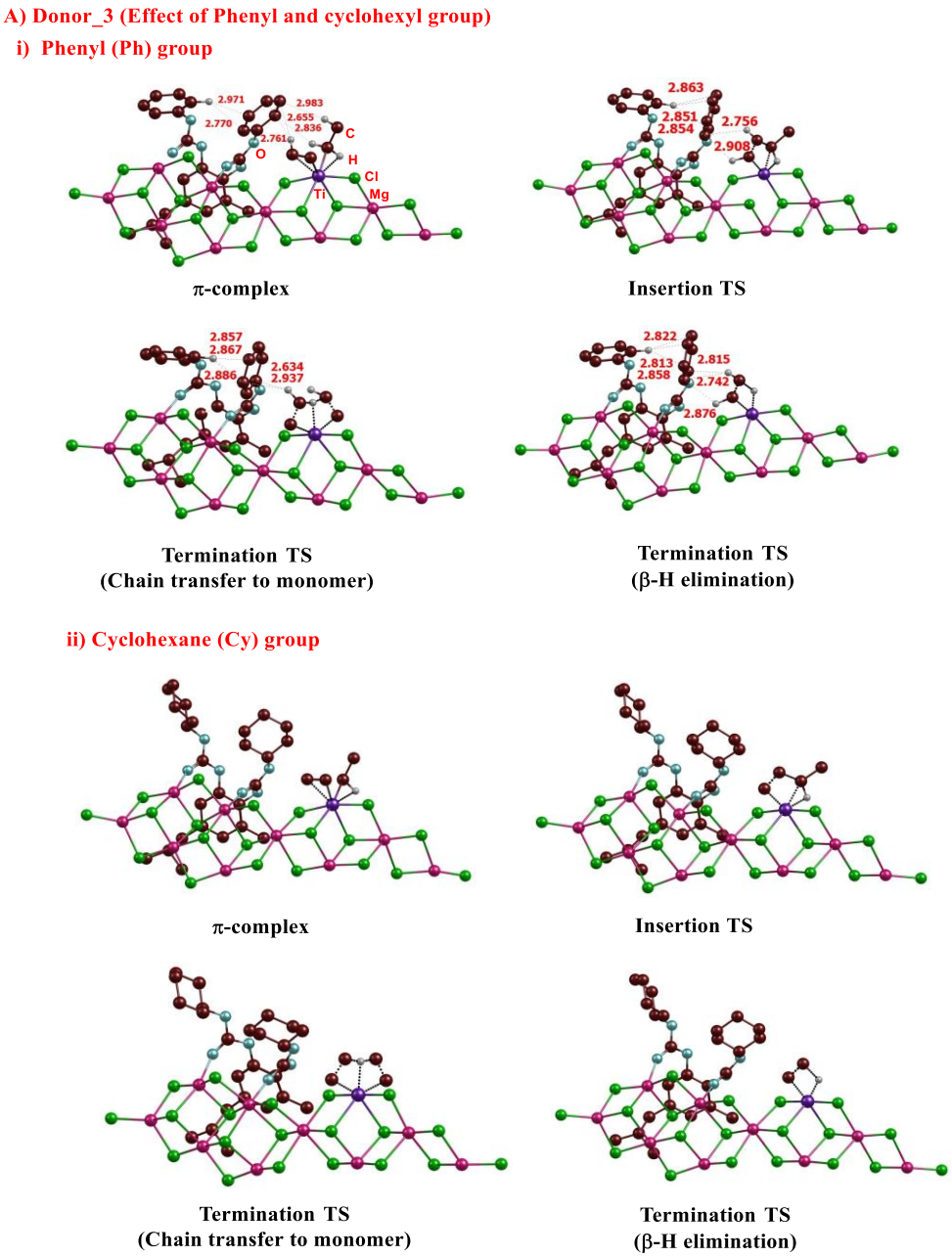

Figure S7. Optimized p-complex and transition state structures for insertion and terminations steps using i) phenyl (Ph) and ii) cyclohexane (Cy) groups on Donor_3: all the $MgCl_2$ layer and hydrogen atoms are not shown for clarity.

Table S2. Ethylene polymerization steps for Donor_3 substituted catalyst systems.

Donor_3 (substituents)	**ΔG (kcal/mol)**				
	π–complex (b)	***Insertion barrier (TS_{b-c})***	***Termination***		***(Lower termination)–(Insertion barriers)***
			Chain transfer to monomer barrier (TS_{b-d})	***β–H elimination barrier (TS_a)***	
Donor_3 (Ph)	–4.4	7.5	17.2	18.0	9.7
Donor_3 (Cy)	1.3	9.1	18.3	19.2	9.2
Donor_3 (Me)	6.2	9.8	18.1	18.0	8.2
Donor_3 (Ph-Ph)	0.2	5.4	12.6	15.4	7.2

iii) Two Methyl (Me) groups

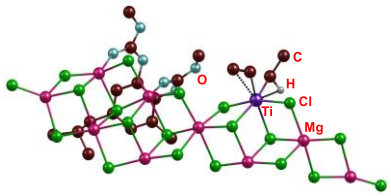

π-complex

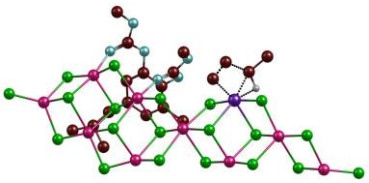

Insertion TS

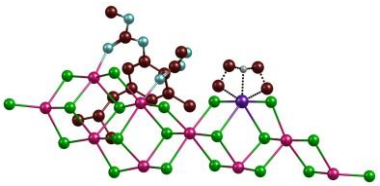

Termination TS
(Chain transfer to monomer)

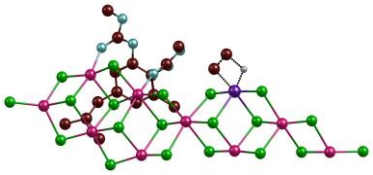

Termination TS
(β-H elimination)

iv) Two biphenyl (Ph-Ph) groups

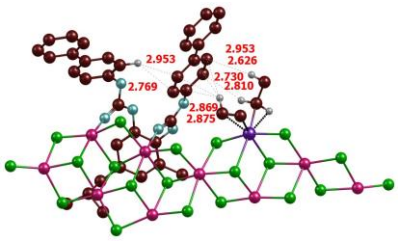

π-complex

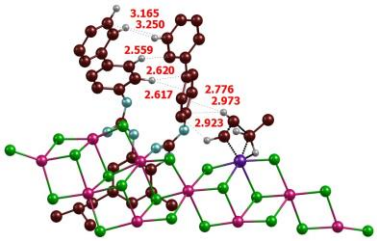

Insertion TS

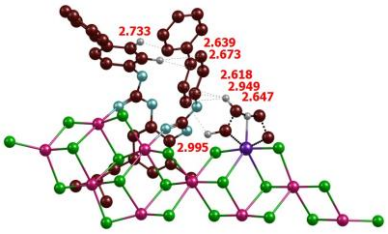

Termination TS
(Chain transfer to monomer)

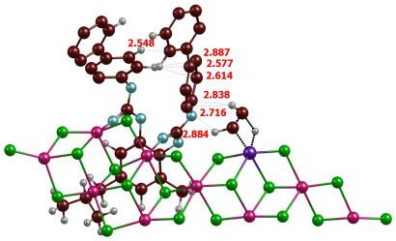

Termination TS
(β-H elimination)

Figure S8. Optimized p-complex and transition state structures for insertion and terminations steps using iii) methyl (Me) and iv) biphenyl (Ph-Ph) groups on Donor_3: all the $MgCl_2$ layer and hydrogen atoms are not shown for clarity.

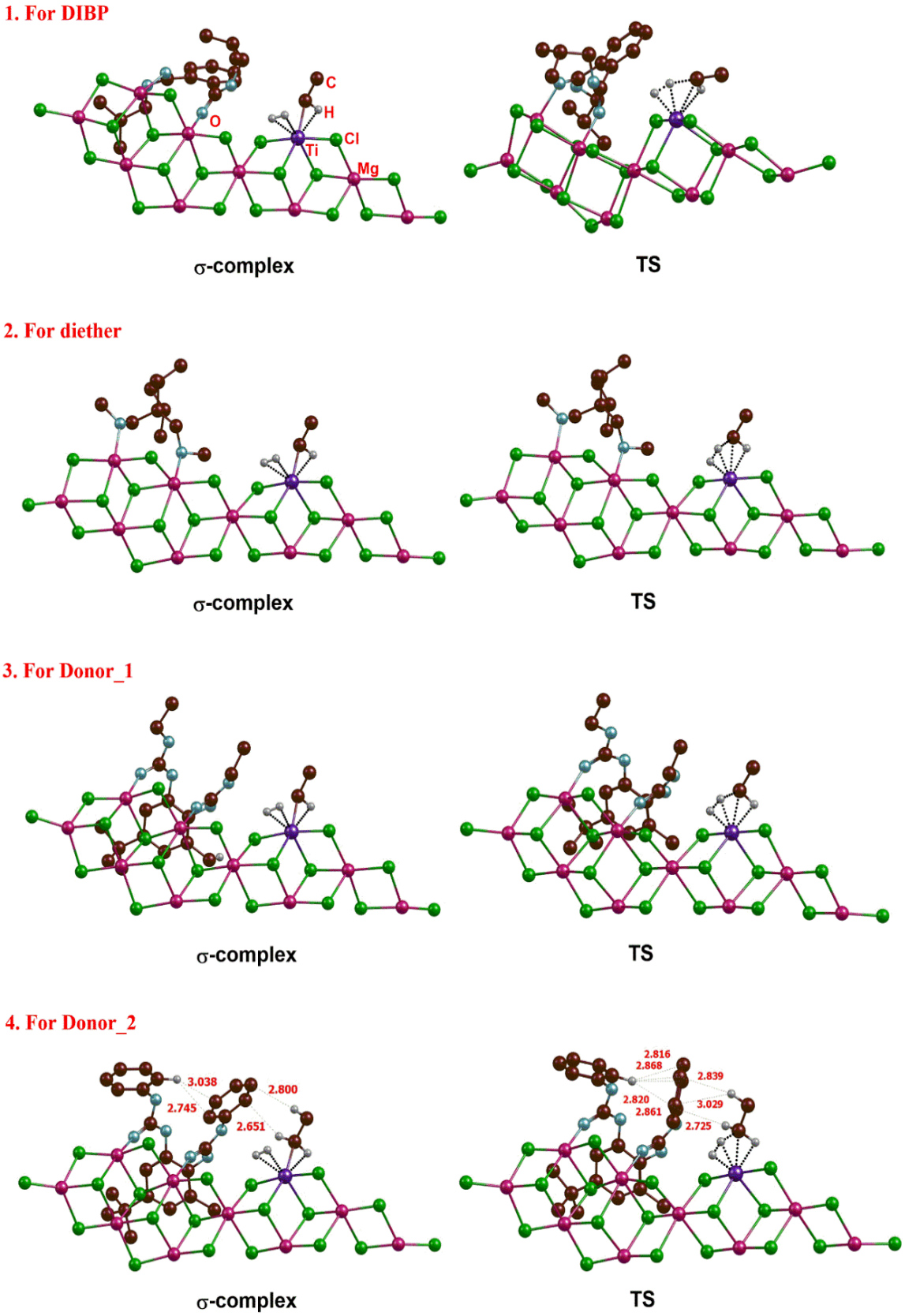

Figure S9. Optimized s-complex and transition state structures for the hydrogen response using DIBP, diether, Donor_1, and Donor_2: all the $MgCl_2$ layer and hydrogen atoms are not shown for clarity.

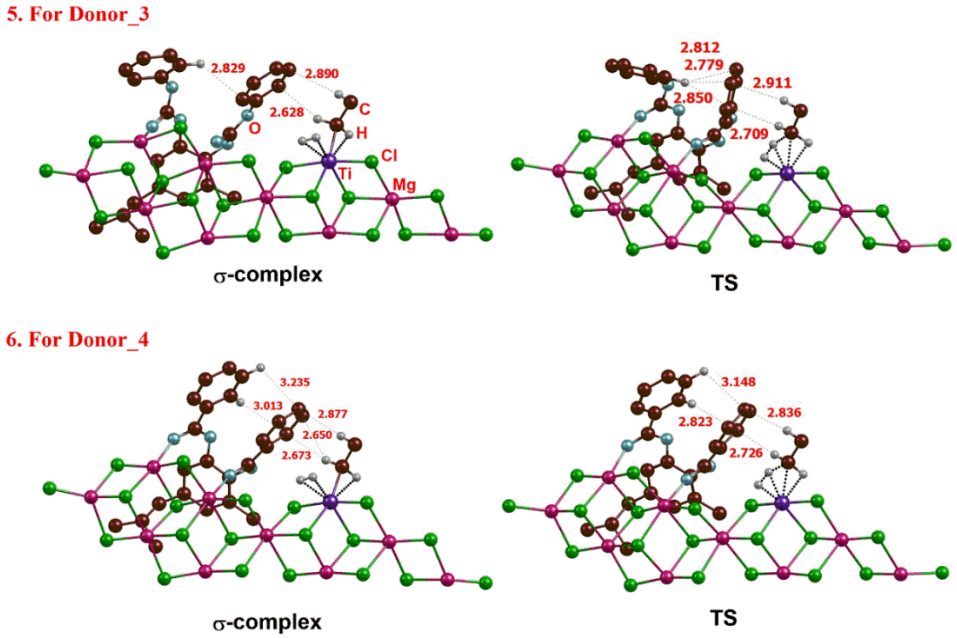

Figure S10. Optimized s-complex and transition state structures for the hydrogen response using Donor_3 and Donor_4: all the $MgCl_2$ layer and hydrogen atoms are not shown for clarity.

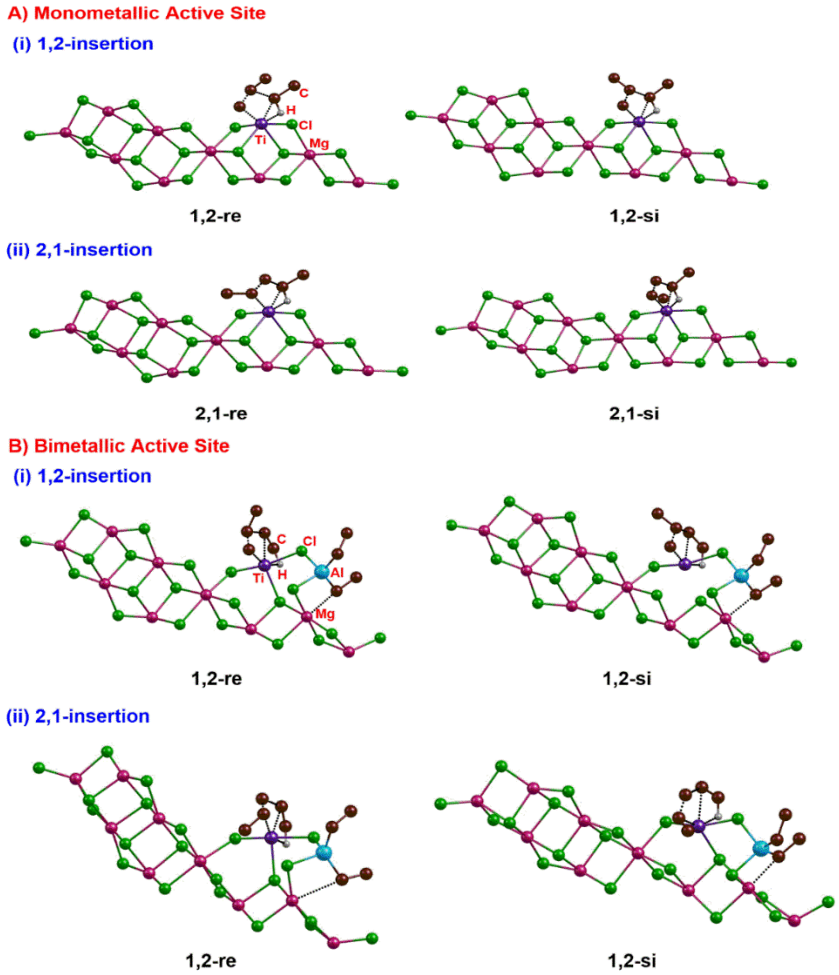

Figure S11. (A and B) Optimized transition state structure for the 1,2- and 2,1-insertion using mono- and bimetallic active site: All the $MgCl_2$ layer and hydrogen atoms are not shown for the clarity.

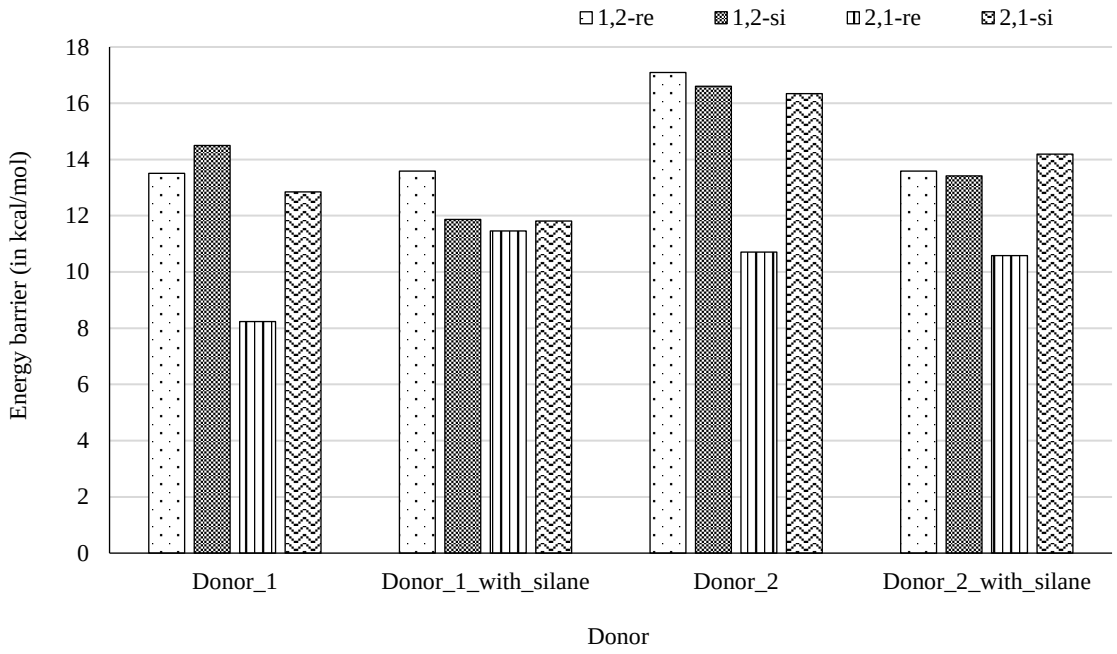

Figure S12. A bar graph for the comparative study of stereoselective behaviour of titanium catalysts using lone Donor_1 and Donor_2 as well as alkoxysilane containing Donor_1 and Donor_2 catalyst systems.

